International Journal of Modern Physics B, Vol. 6, Nos. 3 & 4 (1992) 281–320

ELECTRONIC SPECTRAL AND WAVEFUNCTION PROPERTIES OF ONE-DIMENSIONAL QUASIPERIODIC SYSTEMS: A SCALING APPROACH

HISASHI HIRAMOTO
Department of Physics, College of Humanities and Sciences, Nihon University, Sakurajosui, Setagaya-ku, Tokyo 156, Japan

and

MAHITO KOHMOTO
Institute of Solid State Physics, University of Tokyo, Roppongi, Minato-ku, Tokyo 106, Japan

Received 13 September 1991
Revised 14 November 1991

We review the results of the scaling and multifractal analyses for the spectra and wavefunctions of the finite-difference Schrödinger equation:

$$-\psi_{n+1} - \psi_{n-1} + \lambda V(n\omega)\psi_n = E\psi_n \ .$$

Here V is a function of period 1 and ω is irrational. For the Fibonacci model, V takes only two values (it is constant except for discontinuities) and the spectrum is purely singular continuous (critical wavefunctions). When V is a smooth function, the spectrum is purely absolutely continuous (extended wavefunctions) for λ small and purely dense point (localized wavefunctions) for λ large. For an intermediate λ, the spectrum is a mixture of absolutely continuous parts and dense point parts which are separated by a finite number of mobility edges. There is no singular continuous part. (An exception is the Harper model $V(x) = \cos(2\pi x)$, where the spectrum is always pure and the singular continuous one appears at $\lambda = 2$.)

1. Introduction

In periodic systems, one electron eigenstates are always extended because of Bloch's theorem. In non-periodic systems, on the other hand, the eigenstates exhibit various characters. In particular, random systems have been extensively studied as the Anderson localization problem, and many important properties have been clarified.[1]

Quasiperiodic (QP) systems,[2] which are the subject of this article, are another category of non-periodic systems. Although the QP Schrödinger equations are interesting in themselves, wider attention has been attracted since the discovery of quasicrystals[3,4] which belong to a class of QP systems.

The simplest model to study the electronic properties of the QP systems is a one-dimensional QP tight-binding model (finite-difference Schrödinger equation):

$$-\psi_{n+1} - \psi_{n-1} + \lambda V(n\omega)\psi_n = E\psi_n \ , \tag{1.1}$$

where ω is an irrational number and V is a periodic function, i.e., $V(x+1) = V(x)$. In one-dimensional random systems, it is rigorously proved that the eigenstates are always localized. On the other hand, it is known that the QP systems can have both extended and localized states even in one dimension. Furthermore, "critical" states which may be regarded as being intermediate between localized and extended can appear.

One of the most intensively studied QP systems is the Harper model:

$$V(x) = \cos(2\pi x) \ . \tag{1.2}$$

It is known that all the states are extended for $\lambda < 2$ and all the states are localized for $\lambda > 2$ with an irrational ω.[5] At the critical coupling $\lambda_c = 2$, all the states are critical. Namely, the spectrum of this model is purely absolutely continuous for $\lambda < 2$, purely dense point for $\lambda > 2$, and purely singular continuous for $\lambda = 2$.

In the model defined by

$$V(x) = \tan(2\pi x) \ , \tag{1.3}$$

on the other hand, all the states are localized, irrespective of λ.[6] This is presumably due to the unboundedness of the potential.

Another well-studied example is the Fibonacci model[7,8] defined by

$$\omega = \sigma \equiv \left(\sqrt{5} - 1\right)/2 \ , \tag{1.4}$$

($1/\sigma$ is the golden mean) and

$$V(x) = \begin{cases} -1 & (m - \sigma < x < m) \\ 1 & (m < x < m + 1 - \sigma) \end{cases} \ , \tag{1.5}$$

where m stands for arbitrary integers. The sequence $\{V(\omega), V(2\omega), V(3\omega), V(4\omega), V(5\omega), \ldots\}$ corresponds to the Fibonacci sequence generated by the well-known generation rule ($A \to AB$, $B \to A$). The Fibonacci sequence can be thought of as a one-dimensional version of the quasicrystals. In this model, all the states are critical (purely singular continuous spectrum) for any value of λ.

On seeing the above models, we are apt to consider that the one-dimensional QP models have always pure spectra, i.e., extended, localized and critical states do not coexist in a spectrum. However, this is not the case. The above models are rather special cases. In fact, we have recently found that mobility edges separating extended and localized states in a spectrum can appear in the model defined by[9]

$$\lambda V(x) = \lambda_1 \cos(2\pi x) + \lambda_3 \cos(6\pi x) \ , \tag{1.6}$$

and the model defined by[10]

$$V(x) = \tanh[\mu \cos(2\pi x)] / \tanh \mu \ . \tag{1.7}$$

In this article, we show, mainly following our recent works, that the spectra and the wavefunctions of the one-dimensional QP Schrödinger equations in (1.1) exhibit varieties of properties depending on the form of V.

In order to analyze the spectra and wavefunctions, we adopt a scaling approach. When ω in (1.1) is a rational number M/N (where M and N are integers), the potential is periodic with period N. Thus the spectrum consits of N bands and the wavefunctions are of Bloch type. With increasing N, each band splits into many sub-bands. QP systems are described as a limit of $N \to \infty$. Thus, the spectrum in QP models has a tendency to be a Cantor set. Namely the spectrum consists of infinitely many bands with zero width. We analytically or numerically study asymptotic scaling behaviors of the spectrum and wavefunctions for large N. The wavefunctions are in general classified into two classes: normalizable one and unnormalizable one. The normalizable wavefunction corresponds to a point spectrum, and we call such a wavefunction localized. The unnormalizable wavefunction usually corresponds to an absolutely continuous spectrum which gives a non-singular density of states. We call such a wavefunction extended. However, there can be an unnormalizable wavefunction corresponding to a singular continuous spectrum which gives a singular density of states. We call such a wavefunction critical. We can distinguish localized, extended and critical states through the scaling behavior of the spectrum and the wavefunctions. We employ the multifractal technique developed by Halsey *et al.*[11] to make a systematic analysis of the spectra and the wavefunctions[12] in the formulation of Kohmoto.[13]

The outline of the remainder of this article is as follows. In Sec. 2. we explain the method of the multifractal analysis on the spectra and the wavefunctions of one-dimensional QP systems. Section 3 is devoted to a review of the applications of the multifractal method to the two ideal models: the Harper model and the Fibonacci model. In addition, as an example of physical phenomena reflecting the existence of the critical states, we show the results of the numerical experiments for the time evolution of a wave packet in the Fibonacci model and the Harper model. In Sec. 4. we demonstrate that mobility edges can appear in a spectrum when a model is not so special as the Fibonacci model or the Harper model. Furthermore, we find that critical states hardly appear except for the special cases. In Sec. 5, the stability of the critical states in the Fibonacci model and the critical case of the Harper model against an electron-electron interaction is studied within the mean-field approximation. In the Fibonacci model, the one-body spectrum remains singular continuous when the interaction is not so large. In the Harper model, on the other hand, the singular continuous spectrum disappear no matter how small the interaction is.

2. Scaling Analysis of the Spectra and Wavefunctions

In a scaling analysis of a fractal set with measure (multifractal), we consider a systematic partition of the set. The nth level of the partition consists of a number of bars with length l_i. A scaling index for l_i is given by $l_i \sim e^{-n\varepsilon_i}$. We consider a situation where a probability measure p_i is associated with each bar. The scaling index of the singular measure is given by $p_i \sim l_i^{\alpha_i}$. Now distributions of ε and α specify the scaling properties of the multifractal. Here one can use a formalism equilavent to statistical mechanics to obtain the distributions. The analysis of the spectrum is a special case where we have a distribution of l_i, but where p_i is constant. On the other hand, the wavefunction has a distribution of p_i, but l_i is constant. For a more detailed discussion on the statistical-mechanical formalism of multifractals, see Ref. 13.

2.1. *Spectrum*

In order to understand the scaling of the spectrum, we need to define appropriate scaling indices and the entropy function for them. It is convenient then to consider systematic approximations or finite partitions of the Cantor-set spectrum. This can be done by replacing the irrational number ω by a series of rational numbers which are obtained by truncating the continued-fraction expansion of ω. For example, the inverse of the golden mean $\left(\sigma = \left(\sqrt{5}-1\right)/2\right)$ is approximated by a series of rational numbers $F_{n-1}/F_n = \left\{\frac{1}{2}, \frac{2}{3}, \frac{3}{5}, \frac{5}{8}, \frac{8}{13}, \dots\right\}$ where F_n is a Fibonacci number defined recursively as $F_0 = F_1 = 1$ and $F_{n+1} = F_n + F_{n-1}$. At the nth level of approximation of the Carton-set spectrum, we have N bands whose widths are denoted by $\Delta_i (i = 1, \dots, N)$. The number of bands grows exponentially with respect to n as $N \sim a^n$. In the example above we have $N = F_n$ and $a = 1/\sigma = \left(\sqrt{5}+1\right)/2$.

Let us define a scaling index for Δ_i by

$$\varepsilon_i = \frac{1}{n} \ln \Delta_i \ . \tag{2.1}$$

We also define an entropy function $S(\varepsilon)$ by

$$S(\varepsilon) = \frac{1}{n} \ln \Omega(\varepsilon) \ , \tag{2.2}$$

where $\Omega(\varepsilon)d\varepsilon$ is the number of bands whose scaling index lies between ε and $\varepsilon + d\varepsilon$. Here it is important to notice that Δ_i and $\Omega(\varepsilon)$ depend exponentially on n. A band at the nth level splits into many bands at a higher level and may thus yield a number of different values of the scaling indices ε. However, we expect that the entropy function which represents the distribution of ε will converge to a smooth limiting form as n tends to infinity, and give the complete information about the scaling behavior.

As in the formalism of statistical mechanics, it is convenient to introduce a "partition function" and a "free energy" which are defined by

$$Z_n(\beta) = \sum_{i=1}^{N} \Delta_i^{\beta} \tag{2.3}$$

and

$$F(\beta) = \lim_{n\to\infty} \frac{1}{n} \ln Z_n(\beta) \ . \tag{2.4}$$

Once the free energy is calculated, the entropy function is obtained by a Legendre tansformation,

$$S(\varepsilon) = F(\beta) + \beta\varepsilon \ , \tag{2.5}$$

$$\varepsilon = -\frac{dF(\beta)}{d\beta} \ . \tag{2.6}$$

Thus by changing "temperature" β one can pick a value of ε and then the corresponding $S(\varepsilon)$ is calculated. On the other hand, β can be written in terms of ε as

$$\beta = \frac{dS(\varepsilon)}{d\varepsilon} \ . \tag{2.7}$$

Usually $S(\varepsilon)$ is defined on an interval $[\varepsilon_{\min}, \varepsilon_{\max}]$ and there is no scaling behavior corresponding to ε which is outside the interval and $S(\varepsilon) = 0$. However, $F(\beta)$ is still defined there and from (2.5) it is given by $F(\beta) = -\varepsilon_{\max}\beta$ for $\beta > \beta_{\min}$ and $F(\beta) = -\varepsilon_{\min}\beta$ for $\beta < \beta_{\max}$. Thus useful information is only contained in $F(\beta)$ for the region between $\beta_{\min}$ and $\beta_{\max}$ where it is not linear.

The Hausdorff dimension D_{H} is the zero β_c of the free energy (see (2.3) and (2.4)), i.e.,

$$F(D_{\mathrm{H}}) = 0 \ . \tag{2.8}$$

From (2.5), (2.7), and(2.8) we have

$$\beta_{\mathrm{c}} = \frac{S(\varepsilon)}{\varepsilon} = \frac{dS(\varepsilon)}{d\varepsilon} \ . \tag{2.9}$$

Thus the Hausdorff dimension $D_{\mathrm{H}} = \beta_{\mathrm{c}}$ has a geometrical interpretation in ε-$S(\varepsilon)$ plot: it is a slope of the line through the origin tangent to $S(\varepsilon)$.

The index ε which represents scaling of the Lebesgue measure of the energy spectrum can actually be related to the singular behavior of the density of states. At the nth level of approximation, each band carries the same number of states: $p_i = 1/N = a^{-n}$ (the total number of states is normalized to unity, i.e., $\sum_i p_i = 1$). An index α_i which represents the singular behavior of the density of states is defined as

$$p_i \sim \Delta_i^{\alpha i} \ . \tag{2.10}$$

Since $p_i = 1/N = a^{-n}$ and $\Delta_i \sim e^{-n\varepsilon}$ (see (2.1)), it is related to ε by

$$\alpha\varepsilon = \ln a \ . \tag{2.11}$$

The spectrum of singularity introduced by Halsey *et al.*[11] is given by

$$\Omega'(\alpha) \sim \langle \Delta \rangle^{f(\alpha)} , \tag{2.12}$$

where $\Omega'(\alpha)d\alpha$ is the number of bands whose scaling index α lies between α and $\alpha + d\alpha$, namely $\Omega'(\alpha) = \Omega(\varepsilon)|d\varepsilon/d\alpha|$, and $\langle \Delta \rangle$ is a representative value of Δ which was not specified clearly in Ref. 11. If one identifies $\langle \Delta \rangle = \exp(-n\varepsilon)$ (see (2.1)), $f(\alpha)$ can be related to the entropy function by

$$f(\alpha) = \frac{S(\varepsilon)}{\varepsilon} . \tag{2.13}$$

This simple relation between $f(\alpha)$ and $S(\varepsilon)$ holds since the measure p_i is constant in this case. In general the measure has its own scaling behavior and we do not have a simple relation like (2.13).

An absolute continuous spectrum, for which the states are extended, has a non-singular density of states (apart from possible Van Hove singularities) and α is given by 1 (see (2.10)). On the other hand, a point spectrum, which corresponds to localized states, would give $\alpha = 0$. If α is different from 0 or 1, the spectrum has a nontrivial scaling and one can expect a singular continuous spectrum. The corresponding wavefunctions are neither localized nor extended in the standard way and are called "critical". Thus the entropy functions $S(\varepsilon)$ and $f(\alpha)$ give the essential information on the spectral type and the nature of the wavefunction.

2.2. *Wavefunctions*

A wavefunction is defined on lattice sites which are regular. Therefore the wavefunction is not singular nor fractal as it is. However, for the QP problem there is a consistent way to take a scaling limit of the lattice which is a continuous interval [0,1]. Then the wavefunction defined on the interval can have singularities and scaling which we shall analyze.

In the nth approximation the system is periodic with period N. Consider now the square of the wavefunction at site i as a probability measure, namely,

$$p_i = |\psi_i|^2 . \tag{2.14}$$

We normalize p_i by

$$\sum_{i=1}^{N} p_i = \sum_{i=1}^{N} |\psi_i|^2 = 1 \tag{2.15}$$

for a finite system with N sites. Assign a uniform Lebesgue measure $l = N^{-1}$ to all the sites. Then the size of the system is normalized to unity. In the limit of n tending to infinity, the probability measure is defined on the interval [0,1] and one can discuss singularities and scaling. Here the support of the probability measure is not a fractal, but the distribution of the measure can have scaling. Note the difference from the previous case of the spectrum in which the probability measure is uniformly assigned but the support may be a Cantor set (a fractal).

The scaling index for the Lebesgue measure is given by $l = \exp(-n\varepsilon)$ and is constant:

$$\varepsilon = \ln a \ . \tag{2.16}$$

The scaling index for the probability measure is defined as

$$p_i = l_i^{\alpha} \tag{2.17}$$

and the entropy for α is defined as

$$S'(\alpha) = \frac{1}{n} \ln \Omega(\alpha) \ , \tag{2.18}$$

where $\Omega(\alpha)d\alpha$ is the number of sites which have index between α and $\alpha + d\alpha$. As n is increased a single site is split into a number of sites and it is not possible in general to follow a single scaling index. However we expect that the entropy function $S'(\alpha)$ which represents the distribution of α converges to a smooth limiting form as n tends to infinity. Thus the scaling behavior of the wavefunction is well represented by $S'(\alpha)$. As in the previous case of the spectrum, it is convenient to introduce a partition function

$$Z'_n(q) = \sum_i p_i^q \ , \tag{2.19}$$

and free energy

$$G(q) = \lim_{n \to \infty} \frac{1}{n} \ln Z'_n(q) \ . \tag{2.20}$$

The entropy function is given by the Legendre transformation

$$S'(\alpha) = G(q) + q\alpha\varepsilon \ . \tag{2.21}$$

and

$$\alpha\varepsilon = -\frac{dG(q)}{dq} \ . \tag{2.22}$$

The function $f(\alpha)$ in this case is defined as[11]

$$\Omega(\alpha) \sim l^{f(\alpha)} \ , \tag{2.23}$$

and relates to the entropy function by (see (2.18))

$$S'(\alpha) = \varepsilon f(\alpha) \ . \tag{2.24}$$

For an extended wavefunction we should have $\alpha = 1$, and a localized wavefunction has $f(\alpha)$ consisting of two points: $f = 0$ at $\alpha = 0$ and $f = 1$ at α going to infinity. The point $\alpha = 0$ corresponds to the sites with nonzero ψ_i and the point α at infinity at all the other sites. For a critical wavefunction with a distribution of scaling indices we expect to have a smooth $f(\alpha)$ defined in a finite region $[\alpha_{\min}, \alpha_{\max}]$.

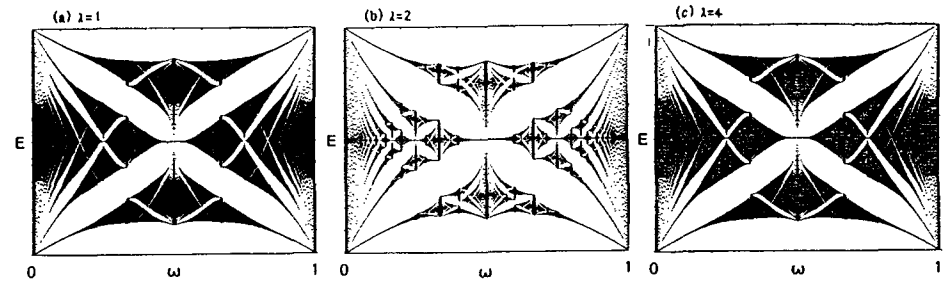

Fig. 1. Spectra for the Harper model with (a) $\lambda = 1$, (b) $\lambda = 2$ and (c) $\lambda = 4$. The energy is normalized appropriately.

3. Models with Pure Spectrum

3.1. *Harper model*

The Harper model defined by (1.1) and (1.2) has been studied for many years in connection with the problem of two-dimensional Bloch electrons in a magnetic field.[14,15] Aubry and Andre[5] showed that this model has a "duality", which means that if the transformation $\phi_m = \sum_n \exp(i2\pi\omega mn)\psi_n$ is made, the Harper equation transforms to the same form with the potential strength $4/\lambda$. Using this duality and Thouless' formula for the Lyapunov exponent,[16] they pointed out that this model with an irrational ω undergoes a metal-insulator transition at $\lambda = 2$. That is, for $\lambda < 2$, all the states are extended, while for $\lambda > 2$, all the states are localized. At the critical point $\lambda = 2$, all the states are critical.

The spectra of the Harper model is shown in Fig. 1 for (a) $\lambda = 1$, (b) $\lambda = 2$ and (c) $\lambda = 4$. The similarity between Fig. 1(a) and Fig. 1(c) is due to the duality discussed above. The wavefunctions at the center and the edge of the spectrum is shown in Figs. 2 and 3. The Harper model is appropriate as the first example of the scaling analysis for the spectrum and the wavefunctions because all the possible types of states, extended, localized and critical, appear depending on λ.[17]

We take ω to be $\sigma \equiv (\sqrt{5}-1)/2$. As mentioned in Sec. 2, ω is approached by a series of rational numbers $\omega_n = F_{n-1}/F_n$. In this case, each band for a value of n splits into three sub-bands as n is increased by 2 or 3. Therefore, each point in the spectrum for the irrational limit ($n \to \infty$) (a Cantor set) is specified by an infinite series of 1, 0 and -1, which represent the upper, middle and lower sub-bands, respectively.

First, we show the scaling of the spectrum for several states.[9] When the state under investigation is specified by an infinite sequence $\{C_1\, C_2\, C_3\, C_4\, C_5\, C_6\, C_7\, C_8 \ldots\}$ ($C_j = 1, 0, -1$), we measure the width of the band specified by a finite subsequence $\{C_1\, C_2\, C_3\, C_4 \ldots C_q\}$, which is a band of a periodic system with $N = F_n$. Hereafter, we denote this quantity as B_n. In the notation of the previous section, this is Δ (the Lebesgue measure of the spectrum). We can estimate the spectrum scaling index α

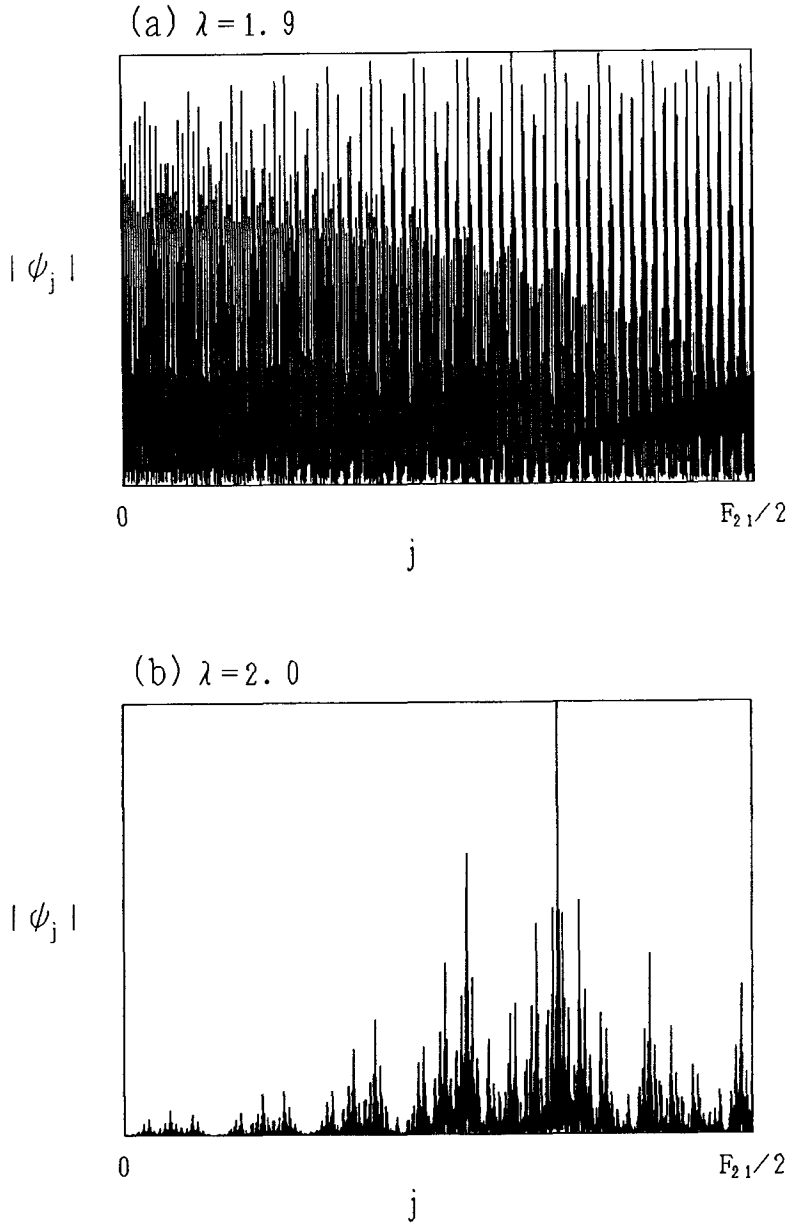

Fig. 2. The wavefunction for the Harper model at the edge of the spectrun with (a) $\lambda = 1.9$, (b) $\lambda = 2.0$ and (c) $\lambda = 2.1$.

in (2.10) by tracing the relation between F_n and B_n (the probability measure p is $1/F_n$).

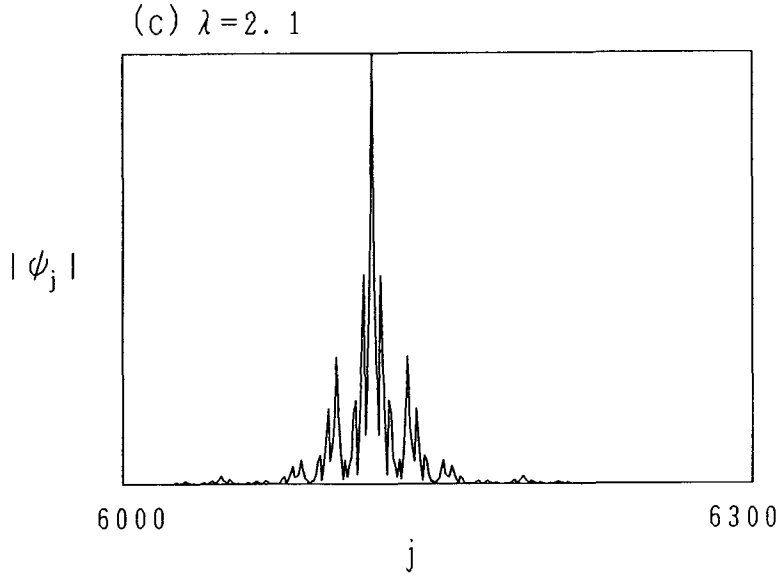

Fig. 2. (*Continued*)

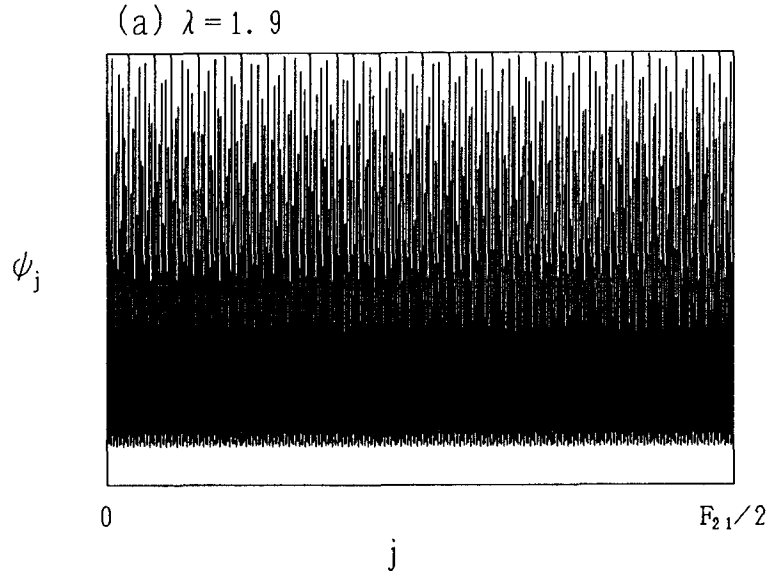

Fig. 3. The wavefunction for the Harper model at the center of the spectrum with (a) $\lambda = 1.9$, (b) $\lambda = 2.0$ and (c) $\lambda = 2.1$.

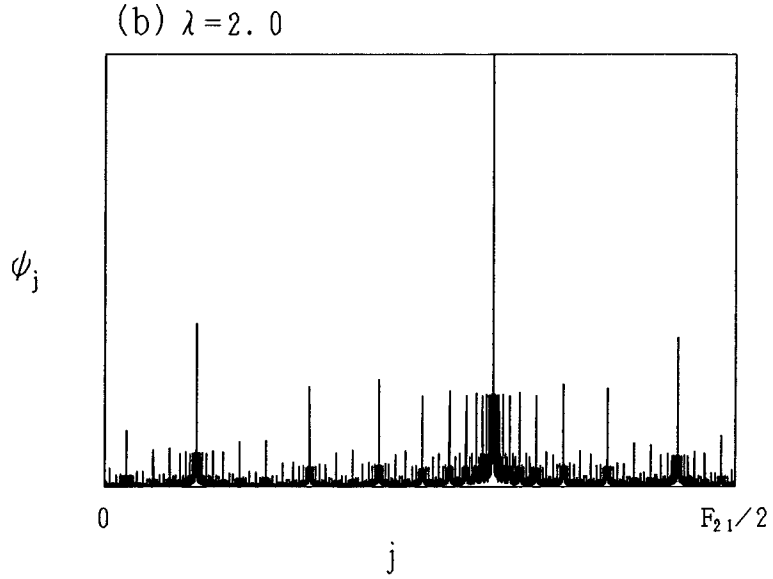

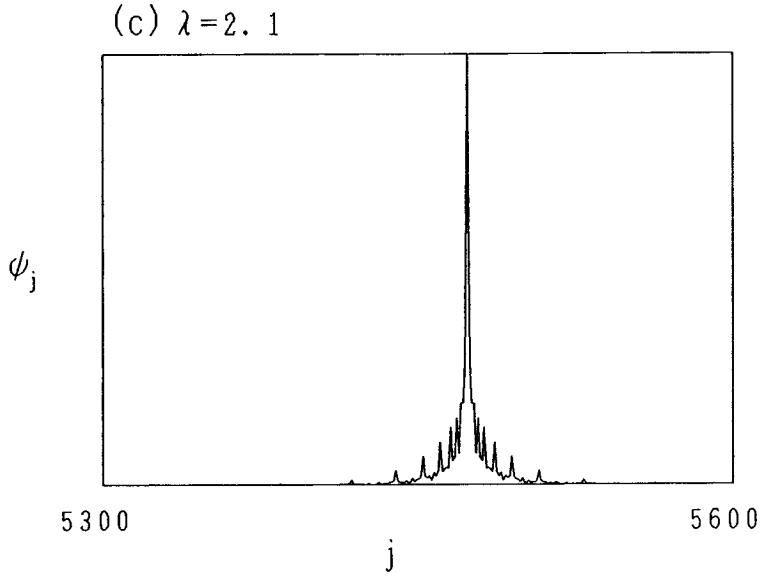

Fig. 3. (*Continued*)

Figure 4 shows plots of F_nB_n versus $n(\approx \ln(F_n)/\ln(1/\sigma))$ for several states with (a) $\lambda = 1.9$, (b) $\lambda = 2.0$, and $\lambda = 2.1$. The states displayed in this figure are (1) $\{0\ 0\ 0\ 0\ 0\ldots\}$ (center of the spectrum), (2) $\{-1\ -1\ -1\ -1\ldots\}$ (edge of the spectrum), (3) $\{0\ -1\ -1\ -1\ -1\ -1\ldots\}$, (4) $\{-1\ 0\ 0\ 0\ 0\ 0\ldots\}$ and (5) $\{-1\ 0\ -1\ 0\ -1\ 0\ -1\ 0\ -1\ldots\}$. For $\lambda = 1.9$, it is observed that $F_nB_n \sim 1$ (i.e., $\alpha = 1$) for (1), (4) and (5), while $F_nB_n \sim 1/F_n$ (i.e., $\alpha = 1/2$) for (2) and (3). This means that all these states are extended. As mentioned in the previous section, the state is extended when $\alpha = 1$. The states (2) and (3) corresponds to "band edges" which are in general identified by $\{C_1\,C_2\ldots1\,1\,1\,1\,1\ldots\}$ or $\{C_1\,C_2\ldots-1\,-1\,-1\,-1\,-1\,-1\ldots\}$. At the "band edges", α is 1/2 when the state is extended. This behavior comes from a remnant of Van Hove singularities in one-dimensional bands.

For $\lambda = 2.0$, the situation is quite different. It is observed that $\alpha = 0.547$ for (1) and (4); $\alpha = 0.421$ for (2) and (3); and $\alpha = 0.513$ for (5). Thus these states are critical at $\lambda = 2.0$. Here is a point to be noted. The states (1) and (4) are governed by the same index, and the states (2) and (3) we also governed by the same index. By investigating other states, we can conclude that all the states specified by $\{C_1\,C_2\,C_3\ldots0\ 0\ 0\ 0\ 0\ 0\ldots\}$ (the "band centers") have an identical value of $\alpha(=\alpha_C = 0.547)$, and all the states specified by $\{C_1\,C_2\,C_3\ldots1\,1\,1\ldots\}$ or

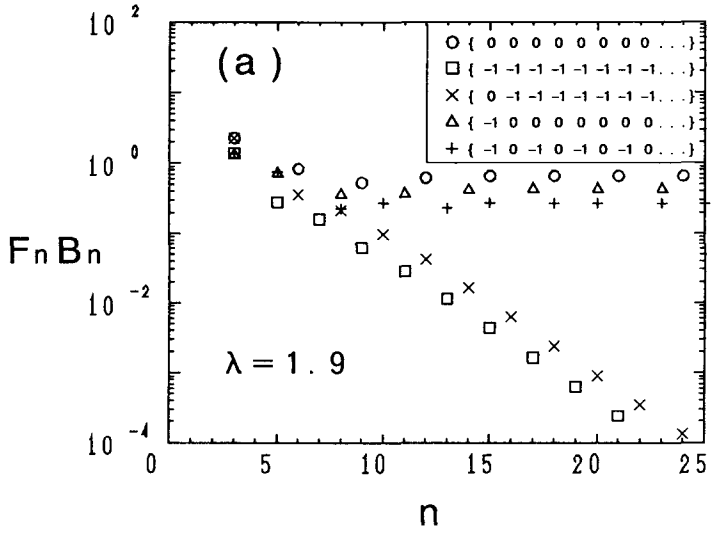

Fig. 4. Plots of F_nB_n against n for several states of the Harper model with (a) $\lambda = 1.9$, (b) $\lambda = 2.0$ and (c) $\lambda = 2.1$. In (a), the values of α, which is defined by $F_n^{-1} \sim B_n^{\alpha}$, are 1 or 1/2 (a remnant of Van Hove singularity) for all these states; thus they are extended. In (c), α's go to zero; thus all the states are localized. In (b), the values of α are 0.547 for the states $\{\ldots0\ 0\ 0\ 0\ 0\ 0\ldots\}$, 0.421 for the states $\{\ldots-1\ -1\ -1\ -1\ -1\ -1\ldots\}$ and 1.961 for the state $\{-1\ 0\ -1\ 0\ -1\ 0\ -1\ 0\ldots\}$; all these states are critical.

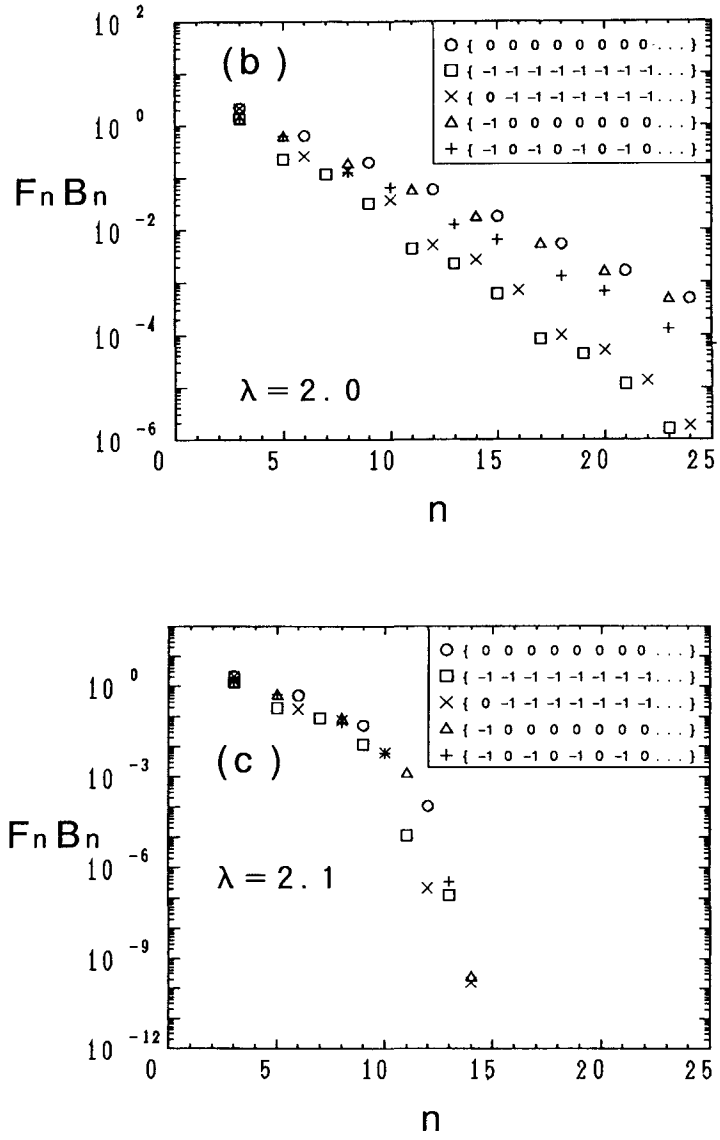

Fig. 4. (*Continued*)

$\{C_1 C_2 C_3 \ldots -1 -1 -1 \ldots\}$ (the"band edges") have an identical value of $\alpha(= \alpha_E = 0.421)$ as well. This situation is the same as the Fibonacci model, where it can be understood from the exact renormalization group (RG).[18] (See also Q. Niu and F. Nori,[19] and T. Dotera,[20] for example.) For the state (5), α takes a value between α_C and α_E.

The fact that all the "edges states" and the "center states" have identical values of α (α_E and α_C) suggests the existence of a renormalization-group structure in the Harper model. In fact, Ostlund and Pandit[21] followed this direction.

For $\lambda = 2.1$, B_n is observed to decrease rapidly for all these states and we have $\alpha = 0$. Thus all these states are localized for $\lambda = 2.1$.

So far we have studied several special states. To confirm that the spectrum is purely absolutely continuous for $\lambda < 2$, purely singular continuous at $\lambda = 2$ and purely dense point for $\lambda > 2$, we must go to a multifractal analysis of the whole spectrum. This was carried out by Tang and Kohmoto.[22] At $\lambda = 2$, the spectrum has a smooth $f(\alpha)$ which has a value on the interval $[\alpha_E, \alpha_C]$ (see Fig. 5). The smooth $f(\alpha)$ shows that the spectrum is purely singular continuous. For $\lambda < 2$, $f(\alpha)$ consists of two points: $f = 1$ for $\alpha = 1$ and $f = 0$ for $\alpha = 1/2$. The point $f = 1$ for $\alpha = 1$ represents that the spectrum is absolutely continuous with a non-zero Lebesgue measure (i.e., the fractal dimension is one), while the point $f = 0$ for $\alpha = 1/2$ represents the remnant of Van Hove singularities as mentioned above. For $\lambda > 2$, $f(\alpha)$ does not converge well in the numerical calculation as the system size increased. This might be a sign of a point spectrum which has localized wavefunctions.

Next we make a multifractal analysis for the wavefunctions.[9] Although this is a direct way to distinguish the extended, localized and critical wavefunctions, we must be deliberate on the finite size effect. A finite system always gives a smooth $f(\alpha)$. Thus, when we numerically calculate $f(\alpha)$ using the formalism in the previous section, it is very important to do an interpolation to $n \to \infty$ from data for finite n's.

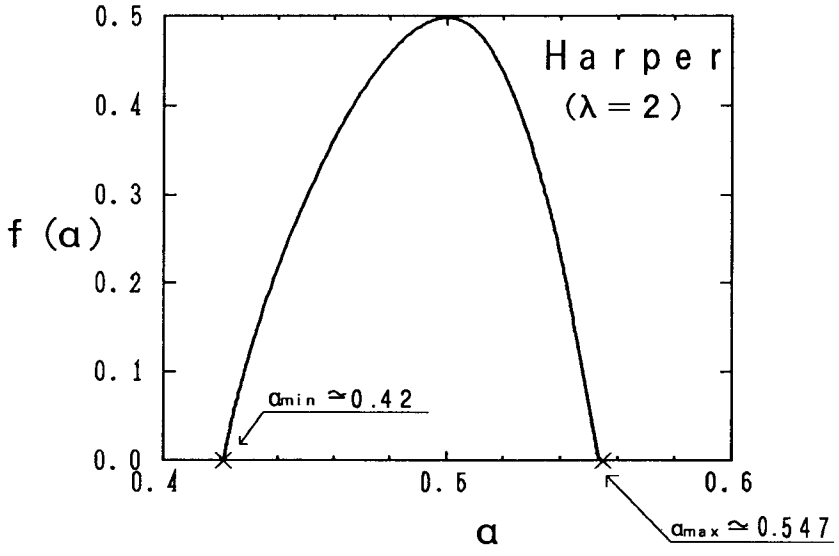

Fig. 5. $f(\alpha)$ for the spectrum of the Harper model with the critical case ($\lambda = 2$).

It turns out that the calculation of $f(\alpha)$ at $\alpha_{\min}$ which represents largest $|\psi_j|^2$'s is most effective in distinguishing the extended, localized and critical wavefunctions. Figures 6(a) and 6(b) are plots of $\alpha_{\min}^{(n)}$ and $f_{\min}^{(n)}$ ($\alpha_{\min}$ and $f(\alpha_{\min})$ calculated for $\omega_n = F_{n-1}/F_n$) against $1/n$ for the wavefunction at the outermost edge of the spectrum $\{-1\ -1\ -1\ -1\ -1\ldots\}$. The following behaviors are clearly seen:

$$f(\alpha_{\min}) = \begin{array}{lll} 1, & \alpha_{\min} = 1 & \text{for an extended state ,} \\ 0, & \alpha_{\min} \neq 0, 1 & \text{for a critical state ,} \\ 0, & \alpha_{\min} = 0 & \text{for a localized state .} \end{array}$$

The leading finite-size correction is $O(1/n)$. This is consistent with the formal analogy between the present method and statistical mechanics in the canonical ensemble formalism (see (2.19) and (2.20); n corresponds to the system size).

At the critical point $\lambda = 2$, $f(\alpha)$ is determined to be a smooth curve and shown in Fig. 7 for the states of (a) the edge of the spectrum $\{-1\,-1\,-1\,-1\,-1\ldots\}$, and (b) the center of the spectrum $\{0\ 0\ 0\ 0\ 0\ldots\}$. The convergence of numerical estimate is good except for the larger side of α (near $\alpha_{\max}$). Notice that this goodness of the convergence is due to the fact that the wavefunctions for (a) and (b) are self-similar. When the wavefunction is "chaotic", the convergence of the numerical data for $f(\alpha)$ is not good. This is similar to the situation in the Fibonacci model.[23] We do not know whether $f(\alpha)$ for the chaotic case converges or not in the infinite limit.

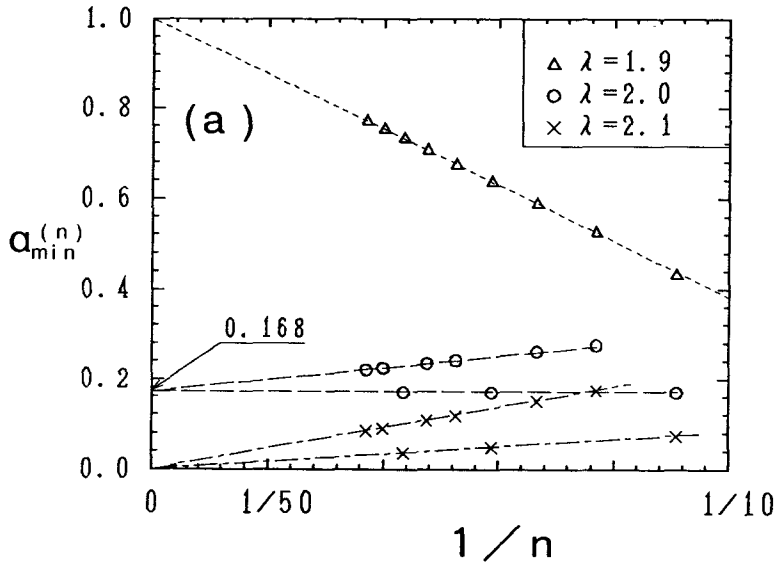

Fig. 6. Plots of (a) $\alpha_{\min}^{(n)}$ and (b) $f_{\min}^{(n)}$ against $1/n$. It is seen that the leading finite-size correction is $O(1/n)$.

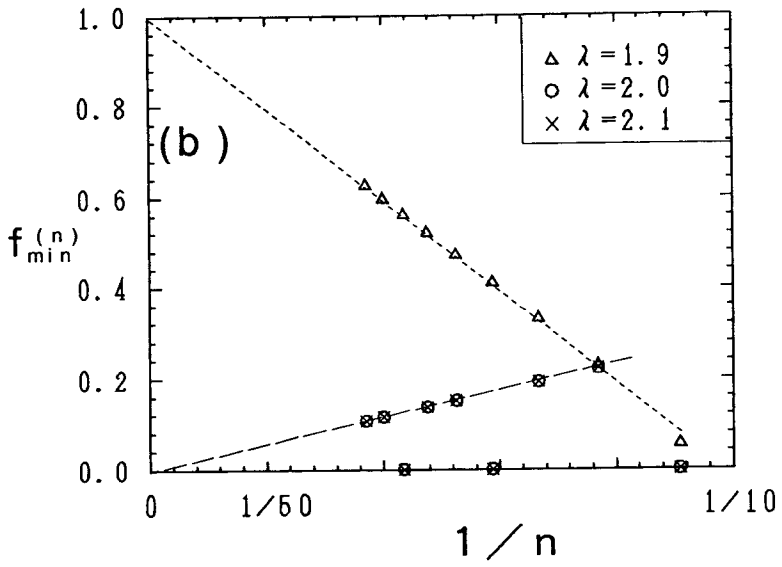

Fig. 6. (*Continued*)

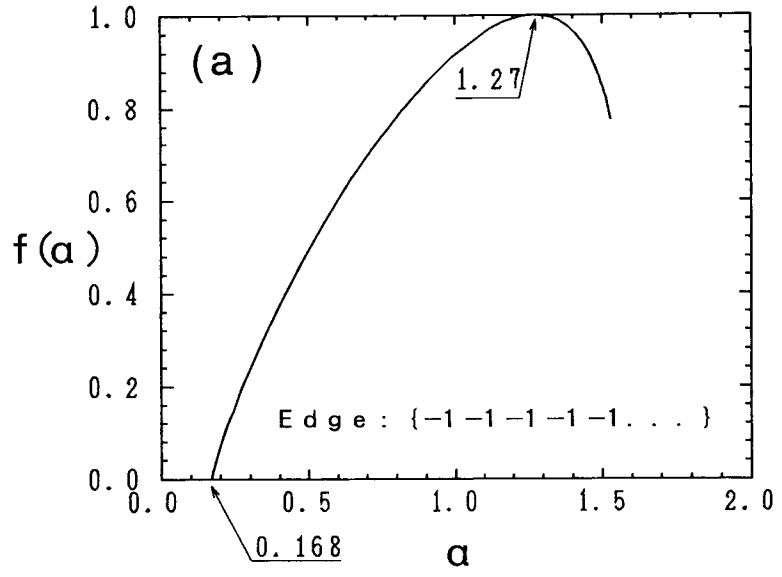

Fig. 7. $f(\alpha)$ for the wavefunctions of the Harper model ($\lambda = 2$) (a) at the edge of the spectrum ($\{-1\ -1\ -1\ -1\ -1 \ldots\}$) and (b) at the center of the spectrum ($\{0\ 0\ 0\ 0\ 0 \ldots\}$).

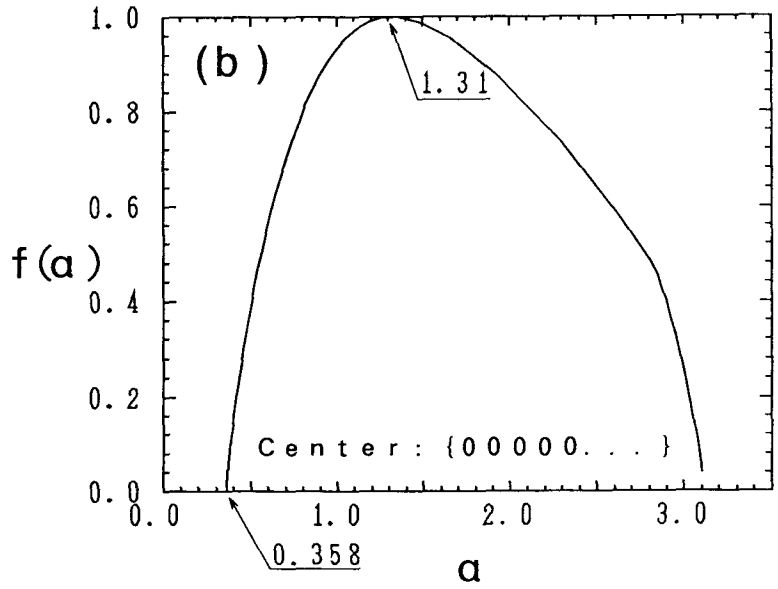

Fig. 7. (*Continued*)

However, we can distinguish the extended, localized and critical wavefunctions by observing the behavior of $\alpha_{\min}$ and $f(\alpha_{\min})$ for large n's.

3.2. *Fibonacci model*

The exact RG transformation[7,8] which is a six-dimensional map exists in the Fibonacci model. It has a three-dimensional sub-map (trace map) and a constant of motion whose value is given by λ^2.[7] The constant of motion determines a two-dimensional non-compact manifold. The points obtained by successive application of the trace map are always on the manifold. The Cantor-set spectrum and its scaling, and purely singular continuous spectrum for any value (except zero) of the potential strength λ was conjectured from the study of the trace map[18] (in fact this conjecture was recently proved rigorously by Suto[24] following the work of Kotani[25]). The scaling of the wavefunctions is also obtained by the study of the full RG map.[26,27] See Ref. 28 for a review.

In this section, we treat the off-diagonal version of the Fibonacci model, which is considered to have the same properties as the diagonal version defined by (1.1), (1.3) and (1.4). The off-diagonal version is written

$$t_{j+1}\psi_{j+1} + t_j\psi_{j-1} = E\psi_j \ , \tag{3.1}$$

where t_j's ($j = 1, 2, \ldots$) take two values t_A and t_B arranged in a Fibonacci sequence T_∞ which is defined as the limit of a recursion $T_{n+1} = T_nT_{n-1}$ with $T_1 = \{A\}$ and

$T_2 = \{AB\}$. So one has $T_3 = \{ABA\}$, $T_4 = \{ABAAB\}$, and so on. In order to investigate the infinite system, we take a series of finite system T_n whose number of sites is a Fibonacci number F_n defined by $F_{n+1} = F_{n-1} + F_n$ with $F_0 = F_1 = 1$.

A multifractal analysis of the spectrum was given by Kohmoto, Sutherland, and Tang.[27] Here we report an exact $f(\alpha)$ for the wavefunction at the center of the spectrum which was obtained by Fujiwara, Kohmoto, and Tokihiro.[23] In order to investigate the wavefunctions on the Fibonacci lattice, (3.1) is written as $\Psi_j = M(t_{j+1}, t_j)\Psi_{j-1}$ with $\Psi_j = \binom{\psi_{j+1}}{\psi_j}$, $\Psi_{j-1} = \binom{\psi_j}{\psi_{j-1}}$ and a transfer matrix $M(t_{j+1}, t_j) = \begin{pmatrix} E/t_{j+1} & -t_j/t_{j+1} \\ 1 & 0 \end{pmatrix}$. A wavefunction is obtained by multiplying Ψ_0 by transfer matrices successively once the energy is taken in the spectrum. There are three types of transfer matrices $M(t_A, t_A)$, $M(t_A, t_B)$, and $M(t_B, t_A)$ (note that there is no successive B's in the Fibonacci sequence). Denote the product of the first F_n transfer matrices by $M^{(n)}$, then we have a RG map

$$M^{(n+1)} = M^{(n-1)}M^{(n)} , \tag{3.2}$$

with $M^{(1)} = B = M(t_A, t_A)$ and $M^{(2)} = A = M(t_A, t_B)M(t_B, t_A)$.[7,8,26]

Let us define $x_n = \mathrm{Tr}\{M^{(n)}\}/2$, then the energy spectrum of a periodic system consisting of T_n's is determined by a condition $|x_n| < 1$. It can be shown[7] that x_n obeys a trace map

$$x_{n+1} = 2x_n x_{n-1} - x_{n-2} . \tag{3.3}$$

The energy E enters in the initial condition and those which give bounded orbits determine the spectrum. In particular, the center of the spectrum has a six cycle[18] and the outermost edge of the spectrum has a two cycle.[27] Most of the bounded orbits, however, are chaotic.

When $E = 0$, not only the trace map (3.3) but also the full RG map (3.2) has a six cycle starting from $B = M(t_A, t_A) = \begin{pmatrix} 0 & 1 \\ -1 & 0 \end{pmatrix}$ and $A = M(t_A, t_B)M(t_B, t_A) = \begin{pmatrix} -R & 0 \\ 0 & -1/R \end{pmatrix}$ with $R = t_B/t_A$.[26] The wavefunction is shown in Fig. 8. This remarkable property allows us to determine $f(\alpha)$ exactly as

$$f(\alpha) = \frac{1}{3\ln\tau}\left[\ln y(R^2 q) - q\frac{d}{dq}\ln y(R^2 q)\right] \tag{3.4}$$

and

$$\alpha = \frac{1}{3\ln\tau}\left[\ln y(R^2) - \frac{d}{dq}\ln y(R^2 q)\right] , \tag{3.5}$$

with

$$y(x) = (1/2x)\left\{(x+1)^2 + \sqrt{(1+x)^4 + 4x^2}\right\} , \tag{3.6}$$

where τ is the golden mean $\frac{\sqrt{5}+1}{2}$. It is plotted in Fig. 9.

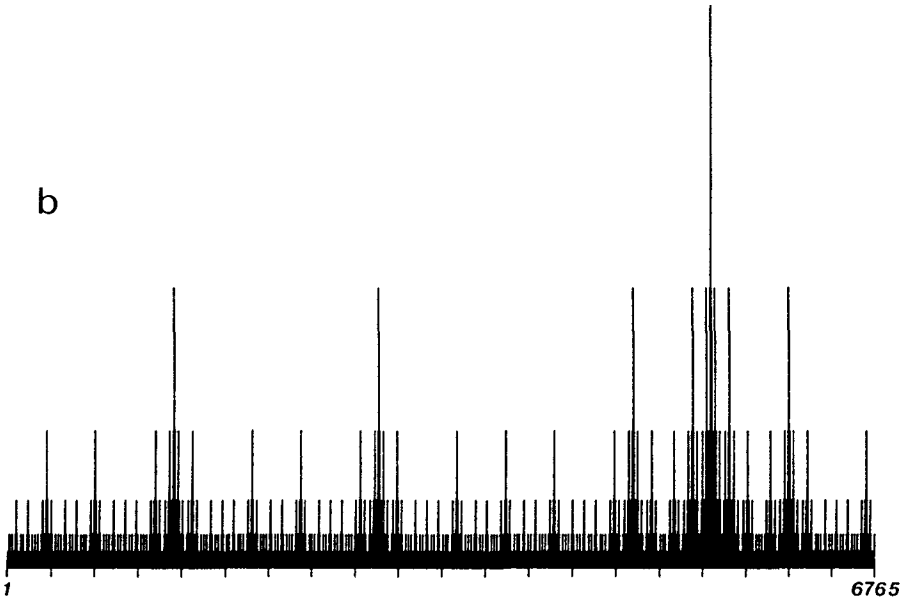

Fig. 8. The wavefunction at the center of the spectrum for the Fibonacci model.

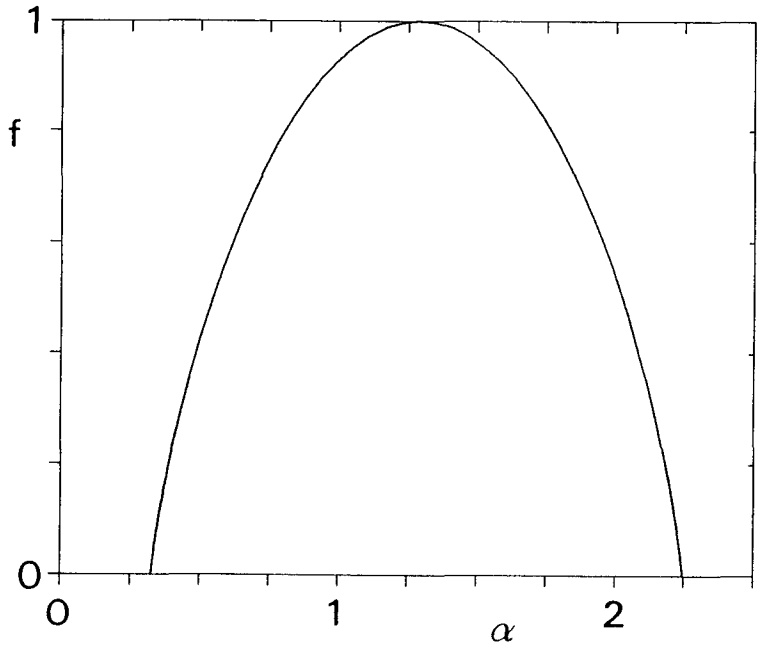

Fig. 9. $f(\alpha)$ for the wavefunction of the Fibonacci model.

The range of α where $f(\alpha)$ is defined is given by $[\alpha_{\min}, \alpha_{\max}] = [1/(3\ln\tau)\{\ln y(R^2) - \ln R^2\}, 1/(3\ln\tau)\{\ln y(R^2) + \ln R^2\}]$, and $f(\alpha) = 0$ for both $\alpha_{\min}$ and $\alpha_{\max}$. The minimum value $\alpha_{\min}$ corresponds to the largest square amplitude of the wavefunction and $\alpha_{\max}$ corresponds to the smallest one. The maximum value of $f(\alpha)$ gives the Hausdorff dimension of the support of the wavefunction. This is as it should be since the support is an interval [0,1] in our formulation. The maximum occurs at $\alpha = \ln y(R^2)/(3\ln\tau)$. It is not difficult to prove that $f(\alpha)$ is symmetric about the maximum as is seen in Fig. 9.

3.3. *Time evolution of wave packets*

As shown above, the Harper model and the Fibonacci model can have critical states (singular continuous spectrum), which do not appear in usual systems (periodic or random systems). Hiramoto and Abe[29,30] carried out numerical experiments on quantum-mechanical diffusion in the Harper model and the Fibonacci model to study what kind of exotic physical phenomena are observed in the systems with singular continuous spectra.

At the time $t = 0$, an electron is placed at a site $n = n_0$, i.e., $\psi_n(t = 0) = \delta_{n,n_0}$. The time evolution of the wavefunction ψ which is governed by the time-dependent Schrödinger equation

$$i\frac{d}{dt}\psi_n = -\psi_{n+1} - \psi_{n-1} + V(n\omega)\psi_n \ , \tag{3.7}$$

is traced. The width of the wave packet is estimated by

$$\sqrt{\langle(\Delta x)^2\rangle} \equiv \sqrt{\sum_n (n - n_0)^2 |\psi_n(t)|^2} \ . \tag{3.8}$$

When the eigenstates are localized, $\sqrt{\langle(\Delta x)^2\rangle}$ remains finite for $t \to \infty$. When the eigenstates are extended, $\sqrt{\langle(\Delta x)^2\rangle}$ increases with increasing t. If we write the overall asymptotic time dependence as

$$\sqrt{\langle(\Delta x)^2\rangle} \sim t^{\gamma} \ , \tag{3.9}$$

γ is 0 for the localized states, while γ is 1 or 1/2 for the extended states. In perfectly periodic systems, the eigenstates are of Bloch type and the motion of an electron is ballistic, i.e., $\gamma = 1$. In three-dimensional random systems with extended eigenstates, the motion is diffusive, i.e., $\gamma = 1/2$. Thus, in usual systems, all the possible values of γ are 0, 1/2 and 1.

In Fig. 10, we show a log-log plot of $\sqrt{\langle(\Delta x)^2\rangle}$ vs. t for the Fibonacci model with several values of λ. The overall behavior of these curves are well fitted by (3.9). In contrast to the usual systems (periodic or random), however, the index γ continuously decreases from 1 to 0, accordingly as λ is increased as shown in Fig. 11.

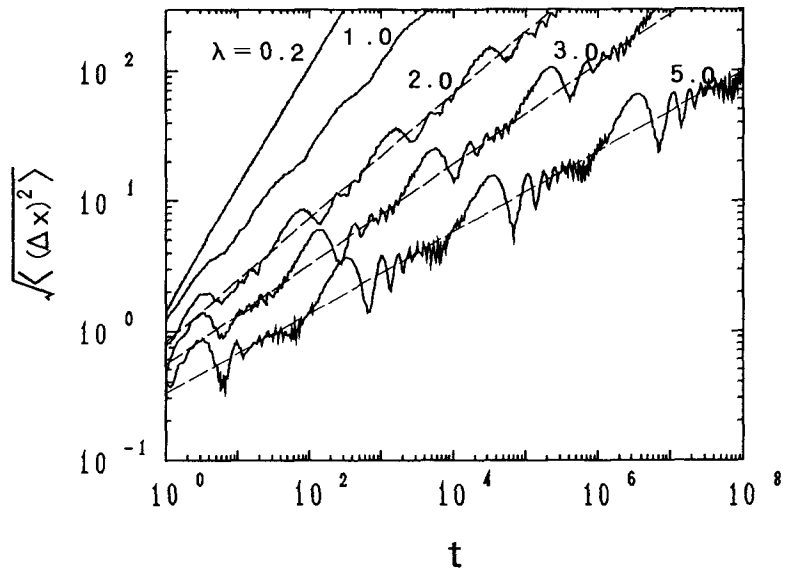

Fig. 10. Plot of the wave packet width $\sqrt{\langle (\Delta x)^2 \rangle}$ as a function of time t for several values of λ in the Fibonacci model. The overall behavior of these curves are expressed by the power-law form (3.9) in the text.

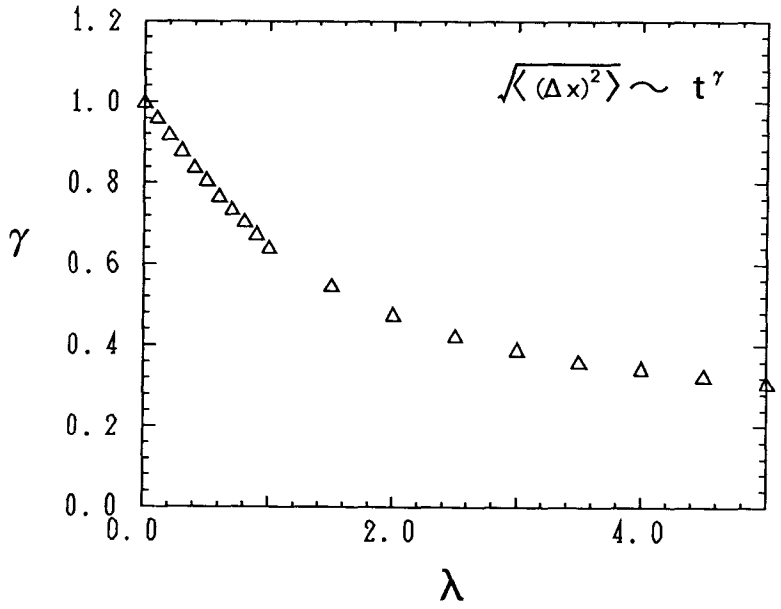

Fig. 11. Plot of the index γ in (3.9) vs. the potential strength λ in the Fibonacci model.

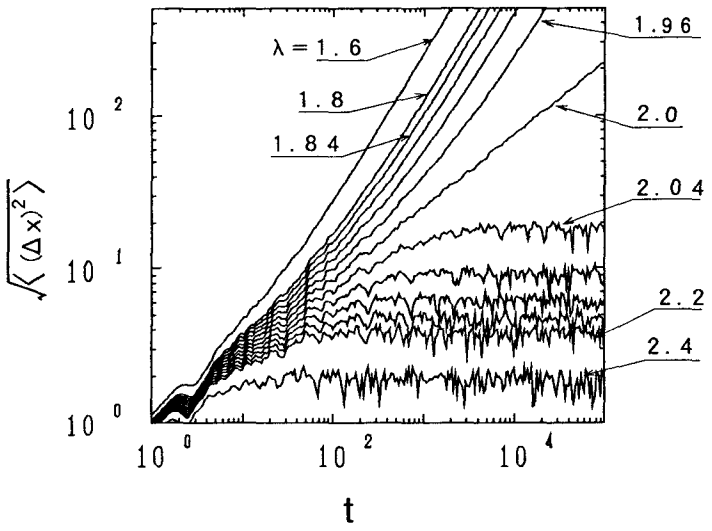

Fig. 12. Plot of $\sqrt{\langle(\Delta x)^2\rangle}$ as a function of t for several values of λ in the Harper model. It turn out that γ is 1 for $\lambda < 2$, 0 for $\lambda > 2$ and 0.485 at $\lambda = 2$.

This anomalous power-law behavior is in striking contrast to that in the systems which have usual extended states and/or localized states.

In Fig. 12 the data for the Harper model with $\omega = \sigma$ is presented. It turns out that γ is 1 (ballistic) for $\lambda < 2$ and is 0 for $\lambda > 2$. In the critical case $\lambda = 2$, γ is about 0.485. These behaviors are consistent with the electronic properties discussed in Sec. 3.1. From these results, we may say that the anomalous power-law "quantum diffusion" is a characteristic feature of the systems with singular continuous spectrum.

4. Models with Non-pure Spectrum

The Fibonacci model and the Harper model treated in Sec. 3 have a remarkable feature: the spectra are pure, i.e., the extended, localized and critical states do not coexist in the spectra. However, this is not a general feature of the one-dimensional QP systems. The purity of the spectra in the Fibonacci model and the Harper model is presumably due to their special forms of $V(x)$. In the Fibonacci model, $V(x)$ takes only two values. In the Harper model, $V(x)$ has only one Fourier component, and as a result, this model has a duality.

In this section, we study more general models and demonstrate that non-pure spectra can appear. Once we know that the non-pure spectra can appear in the one-dimensional QP models, the next question to be addressed is: what is the structure of the non-pure spectra? One of the possibilities is that the structure would be similar to that of three-dimensional random systems in which localized and extended

states are separated by a finite number of mobility edges in the spectrum. Another candidate for the structure is that there would be infinitely many mobility edges.[5] Since one-dimensional QP systems have in general a topologically self-similar band structure, we may except that every "sub-band" would have mobility edges and there would be an infinite hierarchy of the mobility edges.

It is shown that the non-pure spectra in the one-dimensional QP systems have a finite number of mobility edges at least for the models treated in the following. Further, we see that critical states do not appear except for ideal cases.

4.1. *Generalized Harper model*

When $V(x)$ has a finite number of Fourier components, i.e.,

$$\lambda V(x) = \sum_{p=1}^{n} \lambda_p \cos(2\pi p x) , \tag{4.1}$$

it was proved by Herman[31] that the Lyapunov exponent $\gamma(E)$ satisfies the inequality $\gamma(E) < \ln(|\lambda_n|/2)$ for almost every ω. That is, if $|\lambda_n| > 2$, the Lyapunov exponent $\gamma(E) > 0$ irrespective of E. Thus all the states are exponentially localized. However, this theorem says nothing about the case $|\lambda_n| < 2$.

Hiramoto and Kohmoto[9] numerically studied the model (1.1) with (1.6) in which $V(x)$ has only two Fourier components and ω is $(\sqrt{5}-1)/2$. Similar models have previously been studied by several authors.[5,22,23] Here we review our work in which the appearance of the non-pure spectrum and the precise mobility-edge structure are demonstrated.

Since a relation $V(x+1/2) = -V(x)$ holds as in the Harper model, the spectrum is symmetric with respect to $E = 0$ in the QP limit. Thus, we perform numerical calculations only for $E \leq 0$. Each point in the spectrum can be specified by an infinite sequence of 1, 0 and -1 as in the Harper model and the Fibonacci model discussed in Sec. 3 because we take $\omega = \sigma \equiv (\sqrt{5}-1)/2$.

When $\lambda_1 = 0$ or $\lambda_3 = 0$, this model reduces to the ordinary Harper model. Thus if $\lambda_1 > 2$ ($\lambda_1 < 2$) and $\lambda_3 = 0$, all the states are localized (extended). If also $\lambda_3 > 2$ ($\lambda_3 < 2$) and $\lambda_1 = 0$, all the states are localized (extended). Furthermore, if $\lambda_3 > 2$, Herman's theorem[31] tells that all the states are localized for any value of λ_1. In the general case ($\lambda_1 \neq 0$ and $\lambda_3 \neq 0$), localized and extended states may coexist.

We show numerical data for $\lambda_1 = 2.0$ and $\lambda_3 = 0.25$ as an example of scaling analysis. First we show the bandwidth analysis. Figure 13 is a plot of n versus $F_n B_n$ for several states. It is clearly seen that the states specified by $\{-1-1-1-1-1-1\ldots\}$, $\{-10000\ldots\}$ and $\{-1111\ldots\}$ are localized, whereas the states specified by $\{00000\ldots\}$, $\{0-1-1-1-1\ldots\}$ are extended. Note that from the plot one sees that the state $\{0-1-1-1-1\ldots\}$ have $\alpha = 1/2$ for the bandwidth scaling index. This is due to the remnant of the Van Hove singularity rather than the critical state (see Sec. 3.1). By applying the same analysis to other states, we can see that all the states specified by $\{0\ldots\}$ are extended and all the states specified

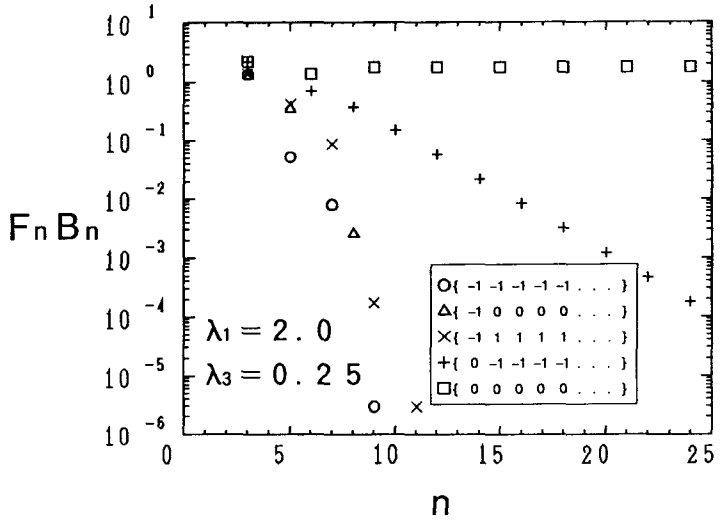

Fig. 13. Plot of F_nB_n against n for $\lambda_1 = 2.0$ and $\lambda_3 = 0.25$. The states specified by $\{-1\ -1\ -1\ -1\ -1\ldots\}$, $\{-1\ 0\ 0\ 0\ 0\ldots\}$ and $\{-1\ 1\ 1\ 1\ 1\ldots\}$ turn out to be localized, while the states specified by $\{0\ -1\ -1\ -1\ -1\ldots\}$ and $\{0\ 0\ 0\ 0\ 0\ldots\}$ are extended.

by $\{1\ldots\}$ or $\{-1\ldots\}$ are localized. Thus the spectrum has two mobility edges located in the gap between the states $\{0\ -1\ -1\ -1\ -1\ldots\}$ and $\{-1\ 1\ 1\ 1\ 1\ldots\}$, and in the gap between the states $\{0\ 1\ 1\ 1\ 1\ldots\}$ and $\{1\ -1\ -1\ -1\ -1\ldots\}$.

Next we show the wavefunction analysis. Figure 14 is a plot of $1/n$ versus (a) $\alpha_{\min}^{(n)}$ and (b) $f_{\min}^{(n)}$ for $\{0\ -1\ -1\ -1\ -1\ldots\}$ and $\{-1\ 1\ 1\ 1\ 1\ldots\}$. It is found that $\alpha_{\min} = \lim_{n\to\infty} \alpha_{\min}^{(n)} = 1$ and $f(\alpha_{\min}) = \lim_{n\to\infty} f_{\min}^{(n)} = 1$ for $\{0\ -1\ -1\ -1\ -1\ldots\}$, while $\alpha_{\min} = 0$ and $f(\alpha_{\min}) = 0$ for $\{-1\ 1\ 1\ 1\ 1\ldots\}$. Thus it is concluded that the states $\{0\ -1\ -1\ -1\ -1\ldots\}$ is extended and the state $\{-1\ 1\ 1\ 1\ 1\ldots\}$ is localized. This is consistent with the bandwidth analysis.

We use both the bandwidth analysis and the wavefunction analysis to obtain the results. We checked that the results obtained from the two methods are always consistent.

Now we show an overall behavior of the spectrum. Figure 15 shows the spectra for various values of λ_1 and $\lambda_3 = 0.25$ fixed. The solid line in the figure represents mobility edges. In the lower energy side of the line, the states are localized, while in the upper side, the states are extended. For $\lambda_1 < \lambda_1^{(c1)}$ (≈ 1.04), all the states are extended and the spectrum is purely absolutely continuous. For $\lambda_1 > \lambda_1^{(c2)}$ (≈ 2.66), on the other hand, all the states are localized and the spectrum is pure point. For $\lambda_1^{(c1)} < \lambda_1 < \lambda_1^{(c2)}$, the spectrum is non-pure: extended states and localized states coexist in the spectrum. At $\lambda_1 > \lambda_1^{(c1)}$, the states of the lowest (highest) energy become localized, and for $\lambda_1 > \lambda_1^{(c1)}$ the mobility edges appear and divide the spectrum into two regions: the states in the outer sides of the mobility edges are

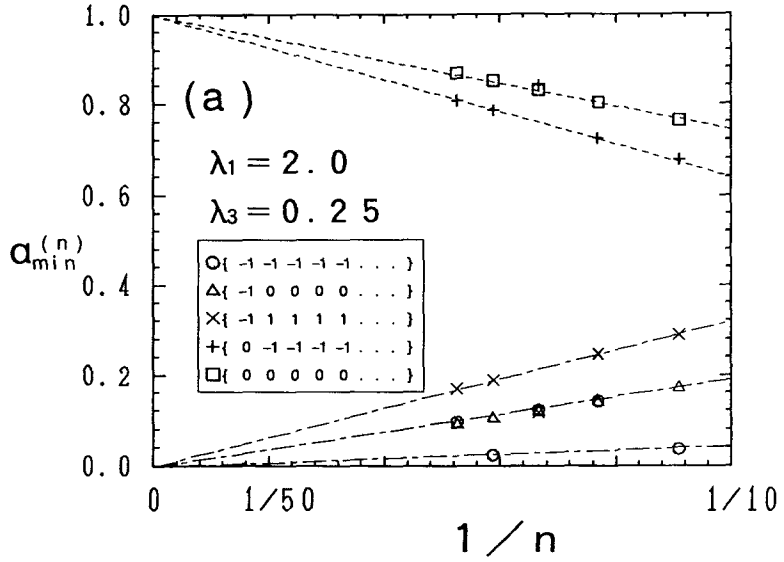

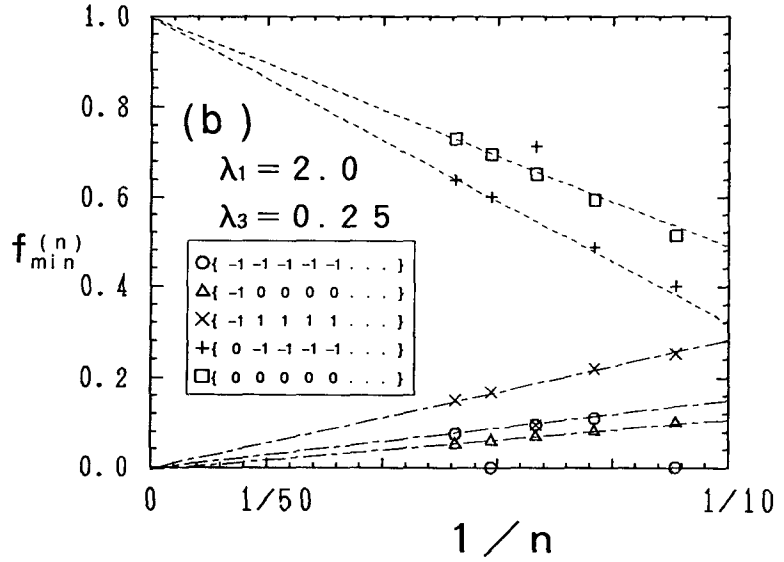

Fig. 14. Plots of (a) $\alpha_{min}^{(n)}$ and (b) $f_{min}^{(n)}$ against $1/n$ for $\lambda_1 = 2.0$ and $\lambda_3 = 0.25$. Localized and extended states are clearly distinguished. The results are consistent with those of the bandwidth analysis in Fig. 13.

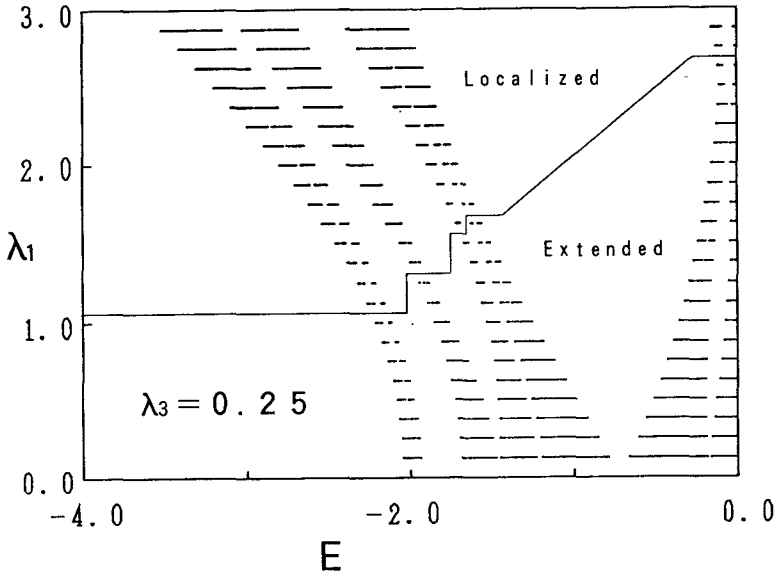

Fig. 15. The energy spectra for various values of λ_1 and $\lambda_3 = 0.25$ fixed.

localized, whereas the states in the inner side are extended. This behavior is similar to the Anderson localization in the three-dimensional random systems. The mobility edges move towards the center of the spectrum as λ_1 is increased, and finally all the states become localized at $\lambda_1 = \lambda_1^{(c2)}$.

In $\lambda_1^{(c1)} < \lambda_1 < \lambda_1^{(c2)}$, the mobility edges have a tendency to locate in a large gap in the spectrum. In Fig. 16, we show how the position of a mobility edge moves with λ_1 when $\lambda_3 = 0.25$. For $1.115 < \lambda_1 < 1.310$, the mobility edge stays in the gap between $\{-1\,-1\,1\,1\,1\,1\,1\ldots\}$ and $\{-1\,0\,-1\,-1\,-1\,-1\ldots\}$, and for $1.355 < \lambda_1 < 1.590$, it stays in the gap between $\{-1\,0\,1\,1\,1\,1\,1\ldots\}$ and $\{-1\,1\,-1\,-1\,-1\,-1\,-1\ldots\}$. In a rather narrow range $1.310 < \lambda_1 < 1.355$, the mobility edge moves between the two large gaps. The situation is similar also in the other narrow regions (for example, $1.04 < \lambda_1 < 1.115$), where we do not show the location of the mobility edge in the figure. In most of the range $\lambda_1^{(c1)} < \lambda_1 < \lambda_1^{(c2)}$, however, the mobility edge stays in the gap between $\{-1\,0\,-\,1\,1\,1\,1\,1\,1\ldots\}$ and $\{-1\,0\,0\,-\,1\,-\,1\,-\,1\,-\,1\,-\,1\ldots\}$ and in the gap between $\{-1\,0\,0\,1\,1\,1\,1\ldots\}$ and $\{-1\,0\,1\,-\,1\,-\,1\,-\,1\,-\,1\,-\,1\ldots\}$.

In Fig. 17 we show the phase diagram obtained from the analysis exemplified above. When λ_1 and λ_3 are sufficiently large, all the states are localized (region I). When λ_1 and λ_3 are small, all the states are extended (region II). In the intermediate values of λ_1 and λ_3, the spectrum is not pure, and mobility edges appear (region III). We find no critical state expect when (λ_1, λ_3) is (2,0) or (0,2).

In this phase diagram, several awkward behaviors are found. The boundary between I and III for $1.5 < \lambda_1 < 3.3$ seems to be precisely $\lambda_3 = 0.5$. A small dip

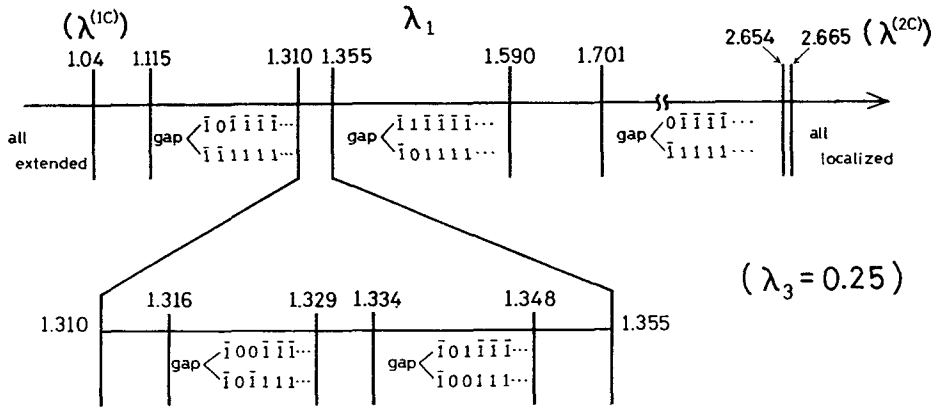

Fig. 16. The location of a mobility edge as a function of λ_1 for $\lambda_3 = 0.25$. When $1.115 < \lambda_1 < 1.310$, for example, the mobility edge is in the gap between $\{-1\ 0\ -1\ -1\ -1\ldots\}$ and $\{-1\ -1\ 1\ 1\ 1\ldots\}$. ($\bar{1}$ in the figure means -1 by the notation in the text).

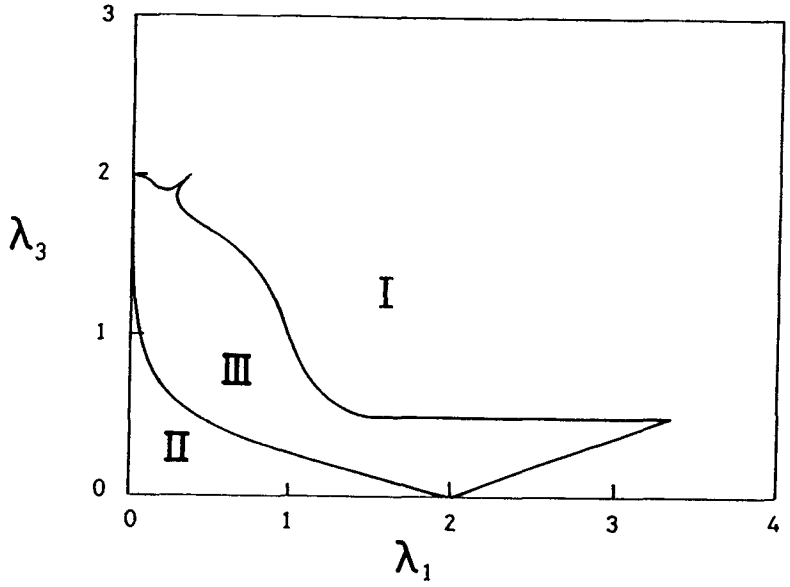

Fig. 17. The phase diagram in the λ_1–λ_3 plain. In region I, all the states are localized, while in region II, all the states are extended. In region III, two mobility edges appear in the spectrum.

appears in the boundary near $(\lambda_1, \lambda_3) = (0, 2)$. These behaviors are probably due to the speciality that $V(x)$ has only two Fourier components. In fact, the model studied in Sec. 4.2 which contains all the higher Fourier components does not show such awkward behaviors.

4.2. *Tanh model*

The periodic function (1.7) ($V(x) = \tanh[\mu \cos(2\pi x)]/\tanh\mu$) gives a model interpolating between the Harper model and the Fibonacci-like model. When μ approaches 0, $V(x)$ approaches $\cos(2\pi x)$, i.e., the model reduces to the Harper model. For $\mu \neq 0$, it contains all the higher Fourier components. Thus it is a smooth modification of the Harper model. When μ goes to infinity,

$$V(x) \to \begin{cases} -1 & (m - 1/4 < x < m + 1/4) \\ 1 & (m + 1/4 < x < m + 3/4) \end{cases} \quad (m : \text{integer}) . \tag{4.2}$$

This function is similar to (1.5) in the sense that $V(x)$ takes only two values.

We show here the result of the scaling analysis when $\omega = \sigma \equiv (\sqrt{5} - 1)/2$ following Ref. 10. First we show an example of the bandwidth analysis for $\mu = 3$ and $\lambda = 1$. Figure 18(a) is a plot of n versus $F_n B_n$ for the states specified by $\{0\ -1\ 1\ C_4\ C_5\ C_6\ C_7 \ldots\}$ ($C_j = -1, 0$ or 1). The states $\{0\ -1\ 1\ -1\ -1\ -1\ -1 \ldots\}$, $\{0\ -1\ 1\ -1\ 0\ 0\ 0 \ldots\}$ and $\{0\ -1\ 1\ -1\ 1\ 1\ 1 \ldots\}$ are extended, whereas the state $\{0\ -1\ 1\ 0\ -1\ -1\ -1\ -1 \ldots\}$ is localized. The same analysis applied to other states

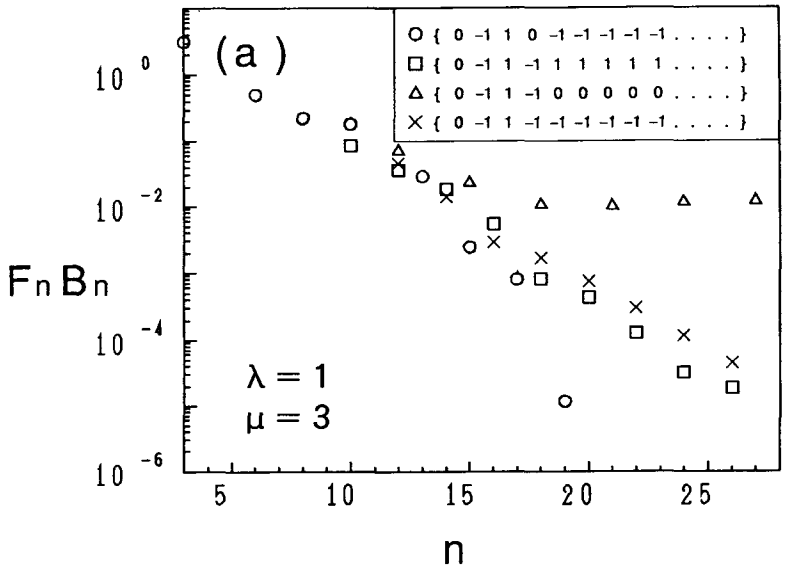

Fig. 18. Plots of $F_n B_n$ against n for $\mu = 3$ and $\lambda = 1$. In (a), a mobility edge is located in the gap between the two states $\{0\ -1\ 1\ 0\ -1\ -1\ -1\ -1\ -1 \ldots\}$ and $\{0\ -1\ 1\ -1\ 1\ 1\ 1\ 1\ 1 \ldots\}$, which are next to each other. In (b), another mobility edge is found in the gap between $\{-1\ -1\ 1\ -1\ 0\ -1\ -1\ -1\ -1 \ldots\}$ and $\{-1\ -1\ 1\ -1\ -1\ 1\ 1\ 1\ 1 \ldots\}$.

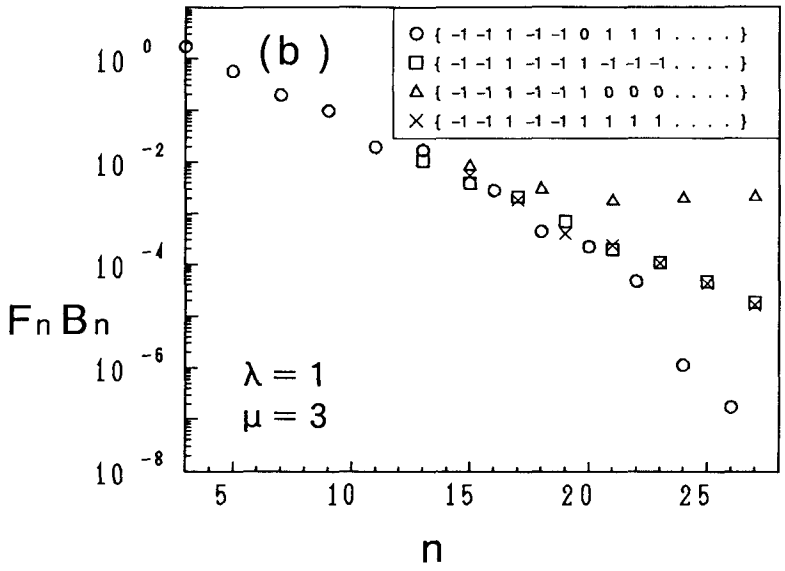

Fig. 18. (*Continued*)

show that all the states specified by $\{0-1\,1-1\,C_5\,C_6\,C_7\ldots\}$ are extended, and all the states specified by $\{0-1\,1\,0\,C_5\,C_6\,C_7\ldots\}$ are localized. Thus there is a mobility edge located in the energy gap between the two states $\{0-1\,1\,0-1-1-1-1\ldots\}$ and $\{0-1\,1-1\,1\,1\,1\,1\ldots\}$, which are next to each other. Figure 18(b) represents the same analysis for the states specified by $\{-1-1\,1-1-1\,C_6\,C_7\,C_8\,C_9\ldots\}$. It is found that another mobility edge is localized in the energy gap between $\{-1-1\,1-1-1\,1-1-1-1-1\ldots\}$ and $\{-1-1\,1-1-1\,0\,1\,1\,1\,1\ldots\}$. No other mobility edge is found for $E<0$. Thus, for $\mu=3$ and $\lambda=1$, there are two mobility edges for $E<0$ (i.e., four mobility edges on the whole spectrum); all the states from $\{0\,0\,0\,0\ldots\}$ to $\{0-1\,1\,0-1-1-1-1-1\ldots\}$ are localized, and all the states from $\{0-1\,1-1\,1\,1\,1\,1\ldots\}$ to $\{-1-1\,1-1\,0-1-1-1-1-1\ldots\}$ are extended, and all the states from $\{-1-1\,1-1-1\,1\,1\,1\,1\ldots\}$ to $\{-1-1-1-1-1-1-1-1\ldots\}$ are localized.

Next we show an example of the wavefunction analysis. Figures 19(a) and 19(b) are plots of $1/n$ versus $\alpha_{\min}^{(n)}$ and $f_{\min}^{(n)}$ for the state $\{-1-1-1-1-1\ldots\}$ at $\lambda=0.76$ and $\lambda=0.77$ with $\mu=3$. It is found that $\alpha_{\min}=\lim_{n\to\infty}\alpha_{\min}^{(n)}=1$ and $f(\alpha_{\min})=\lim_{n\to\infty}f_{\min}^{(n)}=1$ for $\lambda=0.76$, while $\alpha_{\min}=0$ and $f(\alpha_{\min})=0$ for $\lambda=0.77$. Thus it is concluded that the state $\{-1-1-1-1-1\ldots\}$ is extended for $\lambda=0.76$ and localized for $\lambda=0.77$.

The spectra are shown in Fig. 20(a) for $\mu=1$ and Fig. 20(b) for $\mu=3$. As in the generalized Harper model, the localized states and the extended states are separated in the spectra by a finite number of mobility edges. In region I,

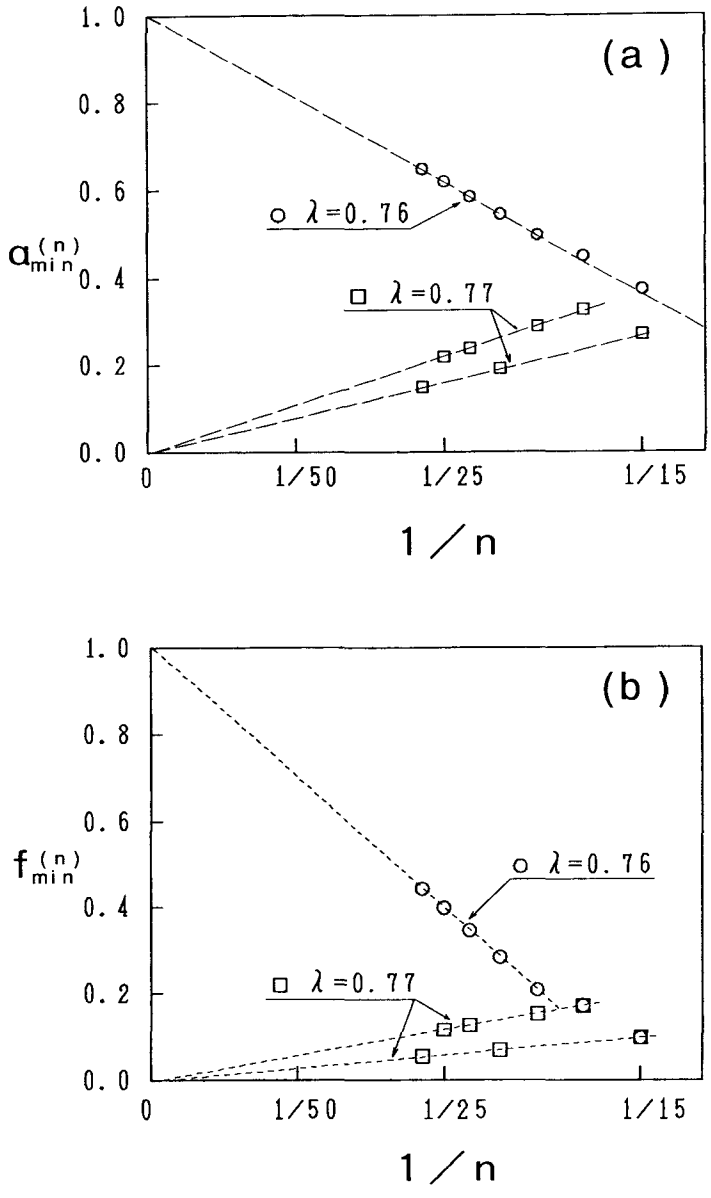

Fig. 19. Plots of (a) $\alpha_{\min}^{(n)}$ and (b) $f_{min}^{(n)}$ as a function of $1/n$ at $\lambda = 0.76$ and $\lambda = 0.77$ with $\mu = 3$ for the state of the spectrum edge $\{-1\ -1\ -1\ -1\ -1\ -1 \ldots\}$.

the spectra are dense points (localized state), while in region II the spectra are absolutely continuous (extended state). They are distinguished by the analyses exemplified above.

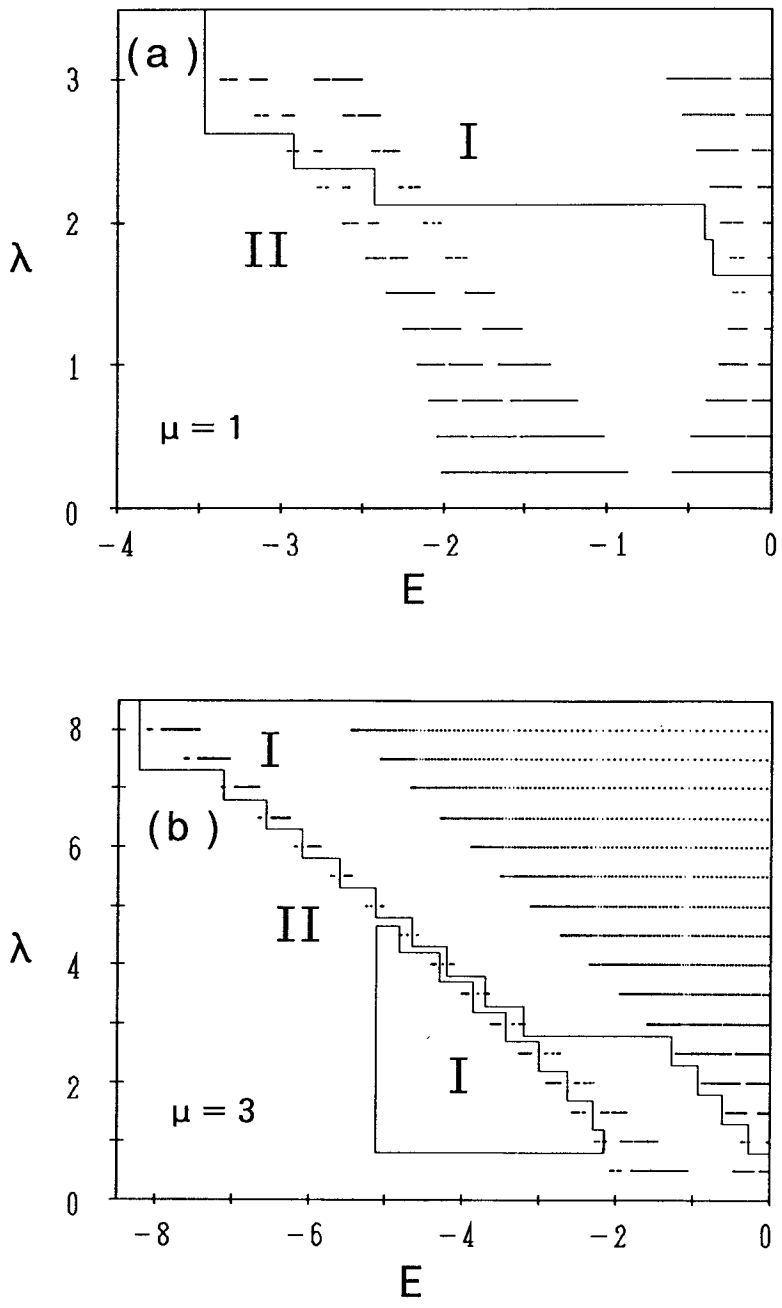

Fig. 20. Spectra of tanh model (1.6) with (a) $\mu = 1$ and (b) $\mu = 3$ for various values of λ. The wavefunctions are localized in region I, and are extended in region II.

One of the most remarkable feature is that the localization of the wavefunctions does not always start from the edge of the spectrum. At small values of λ, all the states are extended for both $\mu = 1$ and $\mu = 3$. For $\mu = 1$, localization takes place first at the center of the spectrum as λ is increased. The boundary between the localized and the extended states (mobility edge) moves from the center towards the edge of the spectrum with increasing λ and finally all the states become localized at a value of $\lambda(= 2.526)$. For $\mu = 3$, a more complicated behavior is found. Localization from the edge of the spectrum occurs in addition to that from the center, and two mobility edges exist for $E < 0$ in a range of λ (i.e., four mobility edges in the whole spectrum). For larger λ, however, the localized states near the edge of the spectrum disappears. In contrast, the region of the localized states around the center gradually extends towards the edge, and finally all the states become localized at $\lambda = 7.28$.

We have also perfomed a calculation for other values of μ. Figure 21 is the phase diagram in the $\mu - \lambda$ plain. In the area below the dashed line, the states near the center of the spectrum is extended; above the dashed line the localized region around the center appears; above the solid line all the states become localized. In the right

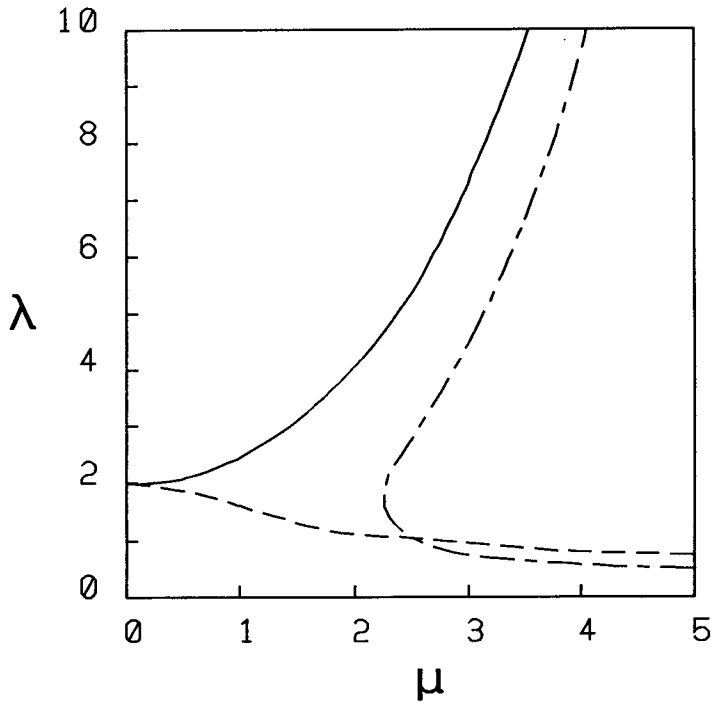

Fig. 21. The phase diagram in the $\mu - \lambda$ plain. Above the solid line all the states are localized. The states at the center of the spectrum is localized (extended) above (below) the dashed line. In the area to the right of the dashed-dotted line, localized states appear near the edges of the spectrum.

area of the dash-dot line, the localized region starting from the edge appears, and there are two mobility edges for $E < 0$. It is an important fact that critical states are not found except for $\mu \to \infty$ or $\mu \to 0$.

The localization starting from the center of the spectrum is in striking contrast to the Anderson localization problem in three-dimensional random systems. A probable explanation of this phenomenon is as follows. In the present model, the probability to find a site with a potential energy near 0 is smaller than that in the Harper model in which all the states localize at once. Conversely, the probability to find a site with a potential energy near $\pm\lambda$ is larger than that in the Harper model. Thus localization is encouraged around the center, while delocalization is encouraged near the edges.

5. Effect of an Electron-Electron Interaction (Mean-Field Approximation)

In this section, we study the effect of an electron-electron interaction within the mean-field approximation.[34] Even if a one-body potential $V(x)$ is an ideal form such as Fibonacci or Harper, the mean field potential may destroy the ideal form. Thus it is reasonable to expect that the one-body spectrum and the one-body wavefunctions in the mean-field approximation should have characters different from those of the Harper model and the Fibonacci model without interactions. The critical states may disappear. Mobility edges may appear.

We treat the Hubbard type on-site interaction:

$$H_{\text{int}} = U \sum_j n_{j\uparrow} n_{j\downarrow} \ , \tag{5.1}$$

where n_{js} is a number operator of an electron with spin s at jth site. We neglect spin polarization, i.e., $\langle n_{j\uparrow} \rangle = \langle n_{j\downarrow} \rangle$ is assumed because our attention is paid to whether the mean field destroys the pure spectrum and the singular continuous spectrum. Thus the suffix s standing for the spin quantum number is omitted hereafter.

The one-body potential at jth site is written as

$$V_{\text{eff}}(j\omega) = \lambda V(j\omega) + W(j\omega) \ , \tag{5.2}$$

where $W(x)$ is a periodic function representing the mean field potential:

$$W(j\omega) = U\langle n_j \rangle \ . \tag{5.3}$$

$W(x)$ is determined self-consistently.

First we study the effect of U on the Fibonacci model. The numerical results shown below are for the Fermi level situated in the first main gap in the spectrum (the gap between $\{-111111\ldots\}$ and $\{0-1-1-1-1-1\ldots\}$. In Fig. 22, a plot of $F_n B_n$ against $1/n$ for several states is displayed for $\lambda = 1$ and $U = 0.5$. It is clear from the figure that these states remain critical. For example, the value of α

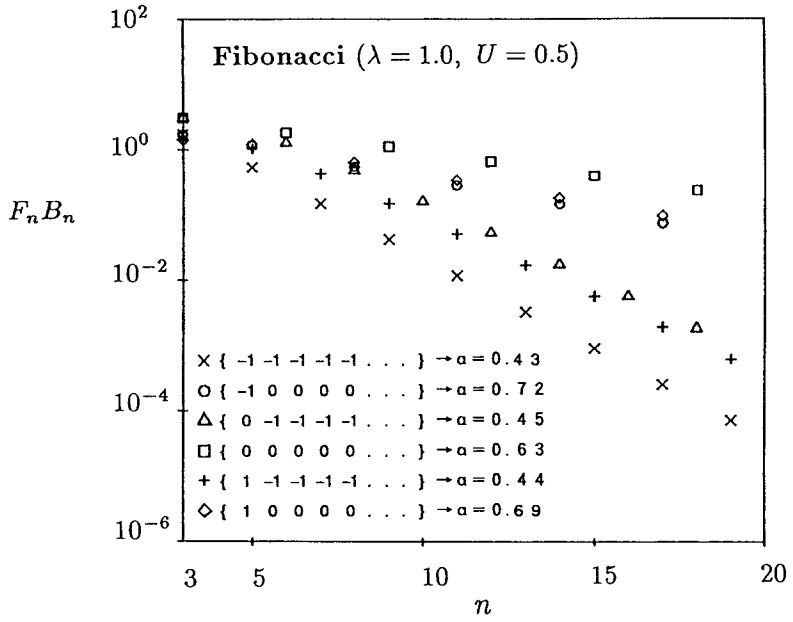

Fig. 22. Plot of F_nB_n as a function of n for the Fibonacci model with the interaction $U = 0.5$. The scaling index α takes various values less than 1; thus the one-body wavefunctions are critical.

($F_{n-1} \sim B_n^{\alpha}$) for the state $\{-1 - 1 - 1 - 1 - 1 - 1 \ldots\}$ is about 0.431. However, this figure shows only that some special states are critical. To investigate whether all the one-body states are critical or not, we must go to a multifractal analysis of the whole spectrum.

Figure 23 shows $f(\alpha)$ for $\lambda = 1$ and $U = 0.5$. This curve is obtained by extrapolating the numerical data, which are calculated by using the formalism in Sec. 2, up to the system size $N = F_{20} = 10946$. The scaling index α distributes continuously between $\alpha_{\min} \approx 0.431$ and $\alpha_{\max} \approx 0.74$. This shows that the mean-field one-body spectrum is a purely singular continuous, i.e., all the one-body wavefunctions are critical.

We have also performed the same analysis for other values of U (including the cases with $U < 0$) and other positions of the Fermi level. The results are as follows. As long as $|U|$ is not so large, the one-body spectrum remains purely singular continuous. When $|U|$ is large, many locally stable solutions appear, and it becomes difficult to obtain the true ground state. Thus we cannot offer any reliable comments for the large $|U|$ case. When the Fermi level is situated in a smaller gap, the threshold value of $|U|$ at which many locally stable solutions appear becomes smaller.

Next we study the effect of U on the Harper model. The location of the Fermi level in the following numerical results is the same as that above (in the first main

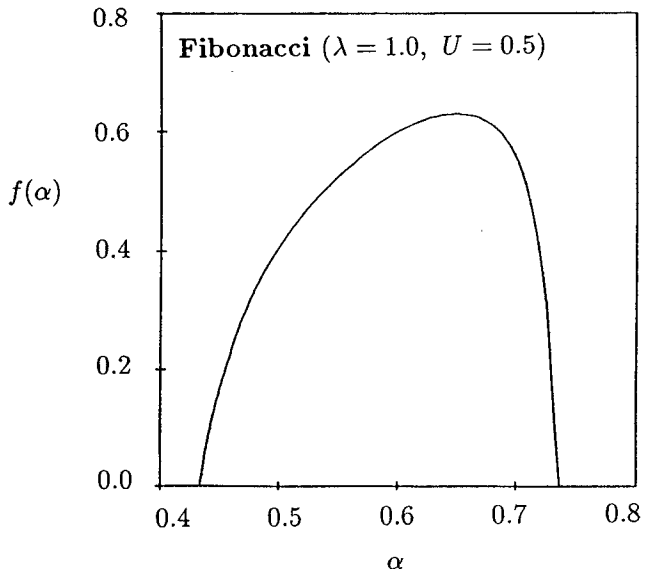

Fig. 23. $f(\alpha)$ of the one-body spectrum for the Fibonacci model with $U = 0.5$. It turns out that the spectrum is purely singular continuous.

gap in the spectrum). The most interesting question is whether the critical states at $\lambda = 2$ are stable against U as in the Fibonacci model or not. Thus, we only show the results for $\lambda = 2$. In Fig. 24, plots of n vs. $F_n B_n$ for several states are shown for (a) $U = 0.5$ and for (b) $U = -0.5$. When $U = 0.5$, we can conclude that the spectrum is purely absolutely continuous, i.e., all the states are extended. When $U = -0.5$, on the other hand, we can show that the spectrum is a purely dense point, i.e., that all the states are localized.

We have systematically investigated the spectrum for various values of U. The result is that the singular continuous spectrum disappears as soon as the electron-electron interaction is added, no matter how small $|U|$ is. However, the purity of the spectrum is not broken for small $|U|$. For $U > 0$, the spectrum is purely absolutely continuous. For $U < 0$, the spectrum is purely dense point.

The phenomenon that the critical states disappear in the Harper model with non-zero U is cosistent with the results of Sec. 4 in which we have studied the one-body problem in various forms of quasiperiodic potentials.

Further, the fact that the states in the Harper model become extended for $U > 0$ and localized for $U < 0$ can be explained as follows. The mean field $W(x)$ defined by (5.3) is expanded as

$$W(x) = \sum_{p=1}^{\infty} W_p \cos(2\pi p x) \ . \tag{5.4}$$

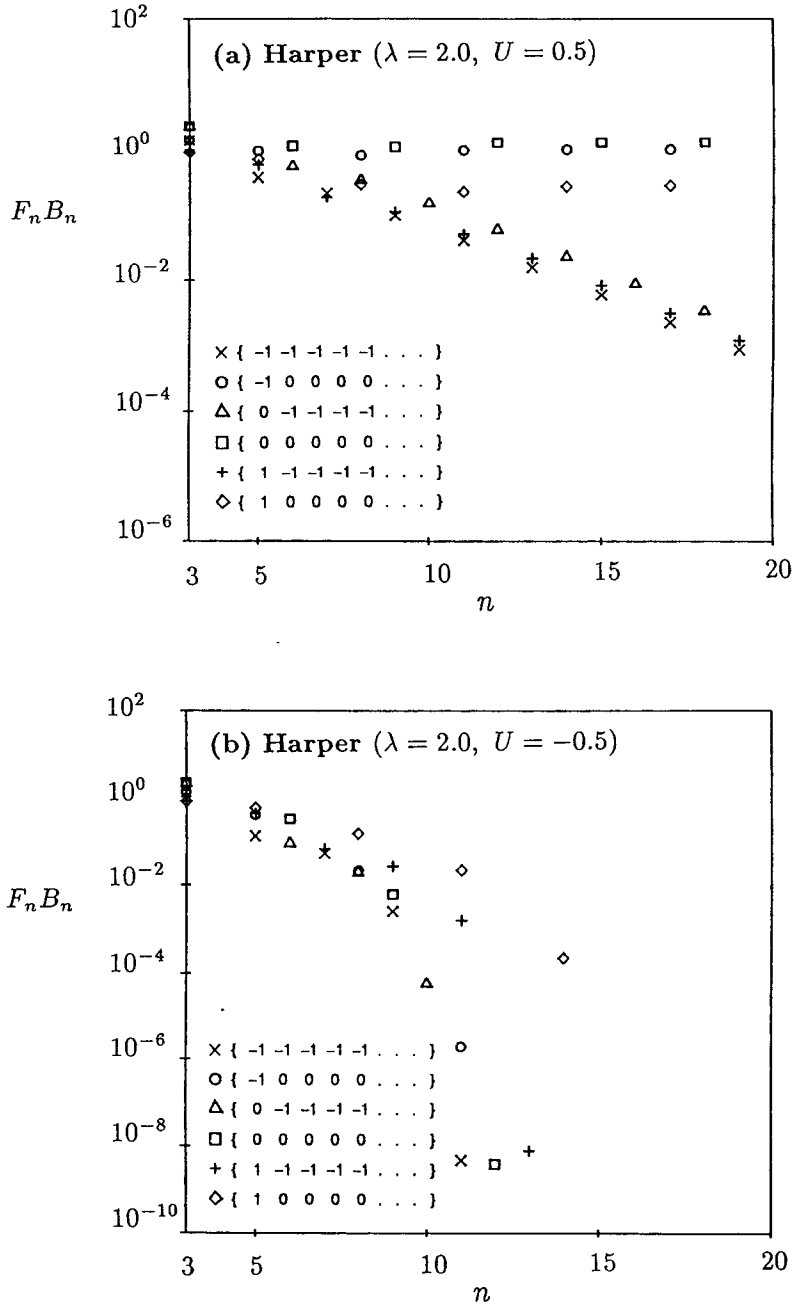

Fig. 24. Plot of $F_n B_n$ as a function of n for the Harper model with (a) $U = 0.5$ and (b) $U = -0.5$

When $U > 0$, the interaction should have the effect of screening of the one-body potential. Thus the first Fourier component W_1 is expected to be negative. If U is small, the higher Fourier components W_p ($p \geq 2$) are small. Thus the mean-field one-body Hamiltonian turns out to be very close to the Harper model with $\lambda = 2 + W_1 < 2$. This is the reason why all the states are extended when U is positive. The localization for $U < 0$ can be explained in the same manner. When U is not small, the higher Fourier components become important, and the non-pure spectrum can appear.

On the other hand, a great surprise is that the states in the Fibonacci model with non-zero U remain critical. Figure 25 is a plot of $W(x)$ calculated self-consistently for $\lambda = 1$ and $U = 0.5$ with the system size $N = F_{20}$. From this figure, it is found that $W(x)$ has steps at $x = n\sigma$ (mod 1), where n is an integer and $\sigma = (\sqrt{5}-1)/2$. As n is increased, the step width of $W(x)$ decreases rapidly; in practice, $W(x)$ seems to be constant except for the steps at several numbers of points $x = n\sigma$ (mod 1). Recently, Kohmoto[33] generalized the simple one-body Fibonacci model to the case of $V(x)$ with a finite number of steps at $x = n\sigma$ (mod 1), and showed that the same dynamical map as that of the Fibonacci model exists. This explains that all the one-body wavefunctions are critical for $W(x)$ in Fig. 25. However, it is an open question why $W(x)$ (the self-consistent mean field) takes such a special form.

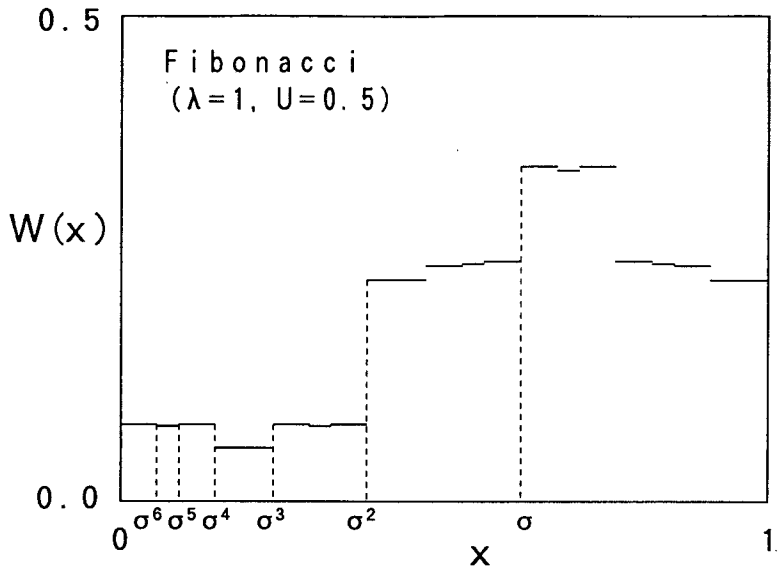

Fig. 25. The mean field $W(x)$ defined by (5.3) in the text. $W(x)$ seems to be constant except for steps at the points $x = n\sigma$ (mod 1), where n stands for arbitrary integers and σ is the inverse of the golden mean.

6. Conclusion

The one-dimensional QP finite-difference Schrödinger equation (tight-binding model) (1.1) can have absolutely continuous, singular continuous, or dense point spectrum depending on the potential strength λ and its form V. The corresponding wavefunctions are extended, critical, and localized, respectively. We have investigated the spectral and wavefunction properties of several models using the scaling and multifractal analyses outlined in Sec. 2.

The Fibonacci model discussed in Sec. 3.2 has a purely singular continuous spectrum, hence critical wavefunctions irrespective of the potential strength λ. For this model the function V takes only two values, i.e., it is constant except for discontinuities.

The Fibonacci sequence is obtained by the generation rule $A \to AB$, $B \to A$. The generalized Fibonacci sequence is obtained by modifying the generation rule, for example, as $A \to A^n B$, $B \to A$. In the generalized Fibonacci models[36–42] V also takes only two values A and B and it seems to have purely singular continuous spectrum. The models where V takes more than two values have also been considered.[35,43,44] We conjecture that if V takes only a finite number of values, then the spectrum is purely singular continuous. In particular, when ω is the inverse of the golden mean σ and V is constant except for steps at $x = -n\sigma \pmod 1$ (n: integer), it is proved that this is the case.[35]

When V is smooth, the situation is quite different. We have investigated the Harper model (1.2), the generalized Harper model (1.6), and the tanh model (1.7) which are in this category. The Harper model is special since it has a duality which maps between the sub-critical region ($\lambda < 2$) and super-critical region ($\lambda > 2$). In the sub-critical region the spectrum is purely absolutely continuous, while it is purely dense point in the super-critical region. At the critical point (self-dual point $\lambda = 2$), the spectrum is purely singular continuous.

In both the generalized Harper model and the tanh model, the spectrum is purely aboslutely continuous for λ small and is purely dense point for λ large. In fact, there are several rigorous theorems for V smooth which support the results for λ small[45–48] and for λ large.[49–53] For an intermediate value of λ, the spectrum is a mixture of absolutely continuous and dense point pieces which are separated by a finite number of mobility edges. They tend to lie in a large energy gap. For the absolutely continuous parts, the band scaling index α defined in Sec. 2.1 is one. The exception, however, exist at band edges where we have $\alpha = 1/2$. The corresponding wavefunction is found to be extended rather than critical. Therefore this singularity can be regarded as a remnant of Van Hove singularity which has $\alpha = 1/2$ in one dimension. The localization seems to start not only from the spectrum edges but also from a portion of the spectrum where the density of state is small. We did not find any singular continuous parts.

We believe that the generalized Harper model and the tanh model represent the general behaviors for V smooth. Namely, the spectrum is purely absolutely

continuous (extended states) for λ small and it is purely dense point (localized states) for λ large. For an intermediate λ, the spectrum is a mixture of absolutely continuous parts and dense point parts which are separated by a finite number of mobility edges. There is no singular continuous part. The exception is the Harper model where it has a singular continuous spectrum (critical states) at the critical point $\lambda = 2$. This is due to the special duality of this model. Hence a singular continuous spectrum rarely appears for V smooth.[54]

References

1. See, for example, P. Lee and T. V. Ramakrishnan, *Rev. Mod. Phys.* **57**, 287 (1985).
2. See, for example, B. Simon, *Adv. Appl. Math.* **3**, 463 (1982); J. B. Sokoloff, *Phys. Reports* **126**, 189 (1985).
3. D. Schechtman, I. Blech, D. Gratias, and J. W. Cahn, *Phys. Rev. Lett.* **53**, 1951 (1984).
4. D. Levine and P. J. Steinhardt, *Phys. Rev. Lett.* **53**, 2477 (1984).
5. S. Aubry and G. Andre, *Ann. Isr. Phys. Soc.* **3**, 133 (1980).
6. D. R. Grempel, S. Fishman, and R. Prange, *Phys. Rev. Lett.* **49**, 833 (1982).
7. M. Kohmoto, L. P. Kadanoff, and C. Tang, *Phys. Rev. Lett.* **50**, 1870 (1983).
8. S. Ostlund, R. Pandit, D. Rand, H. J. Schellnhuber, and E. D. Siggia, *Phys. Rev. Lett.* **50**, 1873 (1983).
9. H. Hiramoto and M. Kohmoto, *Phys. Rev.* **B40**, 8225 (1989).
10. H. Hiramoto and M. Kohmoto, *Phys. Rev. Lett.* **62**, 2714 (1989).
11. T. C. Halsey, M. H. Jensen, L. P. Kadaoff, I. Procaccia, and B. I. Shraiman, *Phys. Rev.* **A33**, 1141 (1986).
12. T. Janssen and M. Kohmoto, *Phys. Rev.* **B38**, 5811 (1988); T. Janssen and J. Los, *Phase Trans.* **32**, 29 (1991).
13. M. Kohmoto, *Phys. Rev.* **A37**, 1345 (1988).
14. P. G. Harper, *Proc. Phys. Soc. London* **A68**, 874 (1955); D. R. Hofstadter, *Phys. Rev.* **B14**, 2239 (1976).
15. D. J. Thouless, M. Kohmoto, M. P. Nightingale, and M. den Nijs, *Phys. Rev. Lett.* **49**, 405 (1982).
16. D. J. Thouless, *J. Phys.* **C5**, 77 (1972).
17. M. Kohmoto, *Phys. Rev. Lett.* **51**, 1198 (1983).
18. M. Kohmoto and Y. Oono, *Phys. Lett.* **102A**, 745 (1985).
19. Q. Niu and F. Nori, *Phys. Rev. Lett.* **57**, 2057 (1986); Q. Niu and F. Nori, *Phys. Rev.* **B42**, 10329 (1990).
20. T. Dotera, *Phys. Rev.* **B38**, 11534 (1988).
21. S. Ostlund and R. Pandit, *Phys. Rev.* **B29**, 1394 (1984).
22. C. Tang and M. Kohmoto, *Phys. Rev.* **B34**, 2041 (1986).
23. T. Fujiwara, M. Kohmoto, and T. Tokihiro, *Phys. Rev.* **B40**, 7413 (1989).
24. A. Suto, *J. Stat. Phys.* **56**, 525 (1989).
25. S. Kotani, *Publ. Inst. Math. Sci. (Kyoto)*, (1989) No. 692.
26. M. Kohmoto and J. R. Banavar, *Phys. Rev.* **B34**, 563 (1986).
27. M. Kohmoto, B. Sutherland, and C. Tang, *Phys. Rev.* **B35**, 1024 (1987).
28. M. Kohmoto, *Int. J. Mod. Phys.* **B1**, 31 (1987).
29. S. Abe and H. Hiramoto, *Phys. Rev.* **A36**, 5349 (1987); H. Hiramoto and S. Abe, *J. Phys. Soc. Jpn.* **57**, 230 (1988).
30. H. Hiramoto and S. Abe, *J. Phys. Soc. Jpn.* **57**, 1365 (1988).
31. M. Herman, *Commun. Mat. Helv.* **58**, 453 (1983).

32. C. M. Soukoulis and E. N. Economou, *Phys. Rev. Lett.* **48**, 1043 (1982).
33. K. A. Chao, R. Riklund, and Y. L. Liu, *Phys. Rev.* **B32**, 5979 (1985); Y. L. Liu and K. A. Chao, *ibid.* **32**, 8385 (1986); Y. L. Liu and K. A. Chao, *ibid.* **34**, 5247 (1986).
34. H. Hiramoto, *J. Phys. Soc. Jpn.* **59**, 811 (1990).
35. M. Kohmoto, "Dynamical system related to quasiperiodic Schrödinger equations in one dimension", *J. Stat. Phys.*, to be published.
36. S. Ostlund and S. Kim, *Physica Scripta* **9**, 193 (1985).
37. G. Gumbs and M. K. Ali, *Phys. Rev. Lett.* **60**, 1081 (1988).
38. M. Holzer, *Phys. Rev.* **B38**, 5756 (1988); M. Holzer, *ibid.* **B40**, 1709 (1988).
39. F. Wijnands, *J. Phys.* **A22**, 3267 (1989).
40. C. Sire and R. Mosseri, *J. Phys. France* **50**, 3447 (1989); C. Sire and R. Mosseri, *ibid.* **51**, 1569 (1990).
41. M. Kolar and M. K. Ali, *Phys. Rev.* **B41**, 7108 (1990).
42. K. Iguchi, *Phys. Rev.* **B43**, 5915 (1991); K. Iguchi, *ibid.* **B43**, 5919 (1991); preprints.
43. M. K. Ali and G. Gumbs, *Phys. Rev.* **B38**, 7091 (1988).
44. M. Kolar and F. Nori, *Phys. Rev.* **B42**, 1062 (1990).
45. E. Dinaburg and Ya. G. Sinai, *Funct. Anal. Appl.* **9**, 279 (1975).
46. F. Delyon, *J. Phys.* **A20**, L21 (1987).
47. C. Albanese, "Quasiperiodic Schrödinger operators with pure absolutely continuous spectrum", preprint CIMS.
48. L. Eliasson, "Floquet solutions for the one-dimensional quasiperiodic Schrödinger equation", preprint, University of Stockholm.
49. L. Pastur, *Commun. Math. Phys.* **75**, 179 (1980).
50. Ya. G. Sinai, *J. Stat. Phys.* **46**, 861 (1987).
51. V. Chulaevsky and Ya. G. Sinai, *Commun. Math. Phys.* **125**, 91 (1989).
52. J. Fröhlich, T. Spencer, and P. Wittwer, *Commun. Math. Phys.* **132**, 5 (1990).
53. E. Sorets and T. Spencer, "Positive Lyapunov exponents for Schrödinger operators with quasiperiodic potentials", preprint IAS.
54. Another example we are aware of is the modulated spring model (Ref. 12) in which the phonon spectrum is purely singular continuous at the critical coupling (H. Hiramoto and M. Kohmoto, in preparation).